ELSEVIER

Electric forces induced by a charged colloid particle attached to the water–nonpolar fluid interface

Krassimir D. Danov, Peter A. Kralchevsky [*]

Laboratory of Chemical Physics and Engineering, Faculty of Chemistry, University of Sofia, 1164 Sofia, Bulgaria

Abstract

Here, we solve the problem about the electric field of a charged dielectric particle, which is adsorbed at the water–nonpolar fluid (oil, air) boundary. The solution of this problem is a necessary step for the theoretical prediction of the electrodipping force acting on such particle, as well as of the electrostatic repulsion and capillary attraction between two adsorbed particles. In accordance with the experimental observations, we consider the important case when the surface charges are located at the particle–nonpolar fluid boundary. To solve the electrostatic problem, the Mehler–Fock integral transform is applied. In the special case when the dielectric constants of the particle and the nonpolar fluid are equal, the solution is obtained in a closed analytical form. In the general case of different dielectric constants, the problem is reduced to the numerical solution of an integral equation, which is carried out by iterations. The long-range asymptotics of the solution indicates that two similar particles repel each other as dipoles, whose dipole moments are related to the particle radius, contact angle, dielectric constant and surface charge density. The investigated short-range asymptotics ensures accurate calculation of the electrodipping force. For a fast and convenient application of the obtained results, the derived physical dependencies are tabulated as functions of the contact angle and the dielectric constants.
© 2005 Elsevier Inc. All rights reserved.

Keywords: Colloid particles, self-assembly; Electric field of adsorbed particles; Electric-field-induced capillary attraction; Electrodipping force; Interactions between adsorbed charged particles; Particle-stabilized emulsions; Particulate monolayers

1. Introduction

The problem about the interactions of electrically charged colloidal particles adsorbed at an oil–water interface has attracted a considerable attention [1–13] in relation to the properties of particle monolayers [1,2,6,7,11–16], formation of particle-stabilized (Pickering) emulsions [17–21], and colloidosomes [3,22–24].

Especially, it was established that in some cases the adsorbed particles experience a strong lateral repulsion that is insensitive to the addition of electrolyte (up to 1 M NaCl) in the aqueous phase [1,2,6]. It was proven that this effect is due to the presence of electric charges at the particle–oil boundary [1,2,6]. These charges induce a direct electrostatic repulsion between two particles across the oily phase. The latter does not contain dissolved ions, and there the electrostatic interactions are strong and long-range across the oil. Similar effect is observed when the nonpolar fluid is air, instead of oil [8,13].

A charged dielectric particle (silica, glass, latex, etc.), which is located in the oily phase near the phase boundary with water, is attracted by the oil–water interface due to the image-force effect [21]. For the same physical reasons, a particle that is attached to the oil–water interface experiences a normal "electrodipping" force, which pushes it into water [8]. The latter force leads to the formation of a concavity (meniscus, dimple) around the attached particle. The overlap of the menisci around two such particles gives rise to a lateral capillary attraction between them [25,26]. This interaction was termed "electric-field-induced capillary attraction" by Nikolaides et al. [3], who first found out experimentally that ordered particles at the surface of a water drop in oil are confined into potential wells. The presence of wells was explained by the overlap of the capillary attraction and the electrostatic repulsion between two particles [3].
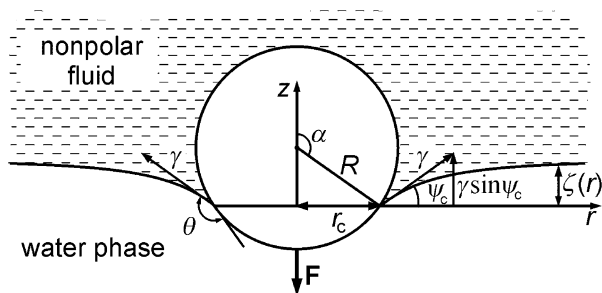
Fig. 1. Sketch of a particle at the interface between water and nonpolar fluid (oil, air). γ is the interfacial tension; R and r_c are the radii of the particle and the three-phase contact line; α and θ are the central and contact angle; ψ_c is the meniscus slope angle at the contact line; $\mathbf{F}$ is a normal force acting on the particle, which can be of electric and/or gravitational origin.

The electrodipping force, $F^{(el)}$, was directly detected in experiments with hydrophobized glass particles floating at the water–tetradecane boundary [8]. The theoretical investigation indicates that this force represents a sum of contributions due to the presence of electric charges at the particle–water, $F^{(w)}$, and particle–nonpolar fluid, $F^{(n)}$, boundaries [8]:

$$F^{(el)} = F^{(w)} + F^{(n)}. \tag{1.1}$$

In experiments with relatively large particles, of radius $R = 200$–300 μm, it has been established that $F^{(el)}$ is insensitive to the concentration of NaCl in the aqueous phase, which means that for the investigated system $F^{(w)}$ is negligible, and $F^{(el)} \approx F^{(n)}$, i.e., the electrodipping force is induced by electric charges at the particle–oil boundary [8].

Theoretical expression for the calculation of $F^{(n)}$ was derived [8]:

$$F^{(n)} = \frac{4\pi}{\varepsilon_n} R^2 \sigma_{pn}^2 (1 - \cos\alpha) f(\alpha, \varepsilon_{pn}), \quad \varepsilon_{pn} \equiv \frac{\varepsilon_p}{\varepsilon_n}. \tag{1.2}$$

Here α is the central angle determined by the position of the contact line on the particle surface (Fig. 1); ε_p and ε_n are the dielectric constants of the particle and of the nonpolar fluid, respectively; σ_{pn} is the surface electric charge density at the particle–oil boundary; the dimensionless function $f(\alpha, \varepsilon_{pn})$ was computed in Ref. [8], by numerical solution of the electrostatic boundary problem, and the numerical results were tabulated (see Table 4 therein).

As illustrated in Fig. 1, the normal force is counterbalanced by the respective projection of the interfacial tension: $F = 2\pi r_c \gamma \sin\psi_c$, where $r_c = R\sin\alpha$ is the contact-line radius, γ is the interfacial tension, and ψ_c is the meniscus slope angle at the contact line. In cylindrical coordinates (r, z), the meniscus profile $z = \zeta(r)$ obeys the Laplace equation of capillarity, which is linearized for the case of small meniscus slope ($\sin^2\psi_c \ll 1$),

$$\frac{1}{r}\frac{d}{dr}\left(r\frac{d\zeta}{dr}\right) - q^2\zeta = \frac{1}{\gamma}p_{el}(r), \tag{1.3}$$

where $q^2 = \Delta\rho g/\gamma$ ($\Delta\rho$, difference between the mass densities of the two phases; g, acceleration due to gravity); $p_{el}(r)$ is pressure (Maxwell stress) exerted at the oil–water interface, which

is induced by the electric field of the charged particle. Equation (1.3) has to be solved along with the boundary conditions $\partial\zeta/\partial r = \tan\psi_c$ at $r = r_c$, and $\zeta = 0$ at $r \to \infty$. In Ref. [8], we determined $p_{el}(r)$ from the numerical solution of the electrostatic boundary problem, and then $\zeta(r)$ was computed by solving numerically Eq. (1.3). In its own turn, the calculation of ζ is a prerequisite for theoretical prediction of the electric-field-induced capillary attraction between two particles. The experiment [3,12,13,15,16,19] indicates that such attraction is really present and plays an important role.

In summary, at present state of the theory, the quantitative description of the basic physical parameters, such as $F^{(n)}$, $p_{el}(r)$, $\zeta(r)$, etc., needs a numerical solution of the electrostatic boundary problem, as described in Ref. [8]. There, an appropriate numerical method was used with a grid of 101×101 subdomains. To verify the latter numerical method, we solved the same problem by using the alternating direction implicit (ADI) method [27] using the general three-level scheme with 2001×2001 subdomains. The results obtained by the two methods were coincident. Although the use of the latter two numerical methods, in principle, solves the problem, their application is time consuming and it demands a corresponding mathematical and computational qualification of the user. It would be much easier if some analytical expressions could be obtained.

In Ref. [8], we proposed a simple semiempirical expression for $p_{el}(r)$,

$$p_{el}(r) = \frac{A_1}{(r - r_c)^{1-\mu} r^{5+\mu}}, \tag{1.4}$$

where A_1 and μ are constants ($0 < \mu < 1$). The parameter μ was determined by fit of experimental data. In general, Eq. (1.4) gives the correct functional dependence of $p_{el}(r)$ at $r \to \infty$ and $r \to r_c$, supposedly μ is accurately determined. However, the comparison with the exact numerical solution for $p_{el}(r)$ shows that Eq. (1.4) is not sufficiently accurate to allow correct computation of $\zeta(r)$ by integration of Eq. (1.3). This is due to the fact that actually A_1 is not a constant, but exhibits some dependence on r.

Our aim in the present paper is to analyze theoretically the electrostatic boundary problem and to derive equations and analytical expressions for the basic physical properties of the investigated system (Fig. 1). The results would allow one to carry out easier and faster calculations of various physical characteristics of the system such as the electrodipping force, $F^{(n)}$; the electric field distribution; the electrostatic interaction between two floating particles; the electric pressure, $p_{el}(r)$, and meniscus profile, $\zeta(r)$, and the electric-field-induced capillary attraction. In other words, our goal in the present paper is to find an alternative and more convenient way for quantitative description of the investigated system, in comparison with the purely numerical approach proposed in Ref. [8].

The paper is organized as follows. In Section 2, the basic equations and boundary conditions are formulated in terms of toroidal coordinates, which correspond to the symmetry of the system. In Section 3, the Mehler–Fock integral transform is applied to solve the problem. In Section 4, a closed analytical solution is obtained for the special case when $\varepsilon_p = \varepsilon_n$. In Sec-

tion 5, the general case, $\varepsilon_p \neq \varepsilon_n$, is considered, and the problem is reduced to the solution of an integral equation. Analytical expressions for the asymptotic behavior of the electric field at short and long distances are derived. In Section 6, the obtained long-range asymptotics is applied to quantify the force and energy of interaction between two adsorbed particles at long distances. The limits of applicability of the present theory and possible extensions are discussed in Section 7. Appendices A, B, and C describe fragments of the theoretical derivations and give details about the computational procedures. The basic physical dependences derived in this study are tabulated in Appendix D. The tables represent an important part of the paper, because they give a possibility the results to be applied without repeating the numerical computations. On the other hand, if one decides to reproduce the developed computational procedures, the tables allow one to test the respective computer programs.

2. Physical system and basic equations

2.1. Equations and boundary conditions

We consider a spherical dielectric particle of radius, R, and dielectric constant, ε_p, attached to the interface between water and a nonpolar fluid (oil, air, etc.); see Fig. 2. As a zero-order approximation, we will assume that the water–nonpolar fluid interface is planar. After determining the electrodipping force and the electric stresses for a flat interface, at the next step one can calculate the interfacial deformation, $\zeta(r)$; see Fig. 1 and Eq. (1.3). The position of the particle at the interface is determined by the central angle, α, which coincides with the three-phase contact angle if the oil–water interface is planar (Fig. 2). In accordance with the frequently used convention, we have $\alpha < 90°$ for hydrophilic particle, and $\alpha > 90°$ for hydrophobic particle.

Our aim is to determine the electric field induced by surface charges, which are located at the particle–nonpolar fluid boundary (S_{pn} in Fig. 2) with density σ_{pn}. In the two dielectric phases, the potential of the electric field obeys the Laplace equation,

$$\nabla^2 \varphi_p = 0 \quad \text{in } \Omega_p \quad \text{and} \quad \nabla^2 \varphi_n = 0 \quad \text{in } \Omega_n, \tag{2.1}$$

where ∇^2 is the Laplace operator; Ω_p and Ω_n are the spatial domains occupied by the particle and the nonpolar fluid,
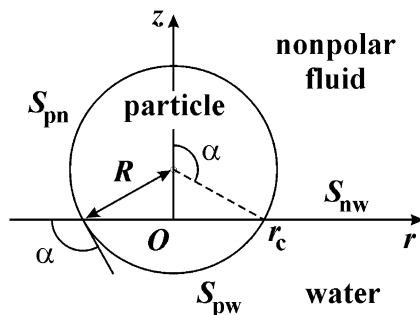

Fig. 2. In zero-order approximation, the water–nonpolar fluid interface, S_{nw}, is planar. S_{pn} and S_{pw} denote the particle–nonpolar fluid and particle–water interfaces, respectively.

respectively. The dielectric constant of water is presumed to be much greater than those of the particle and the nonpolar fluid: $\varepsilon_w \gg \varepsilon_p, \varepsilon_n$. For this reason, the electric field created by charges, located in the nonpolar phases, practically does not penetrate into the water phase; see, for example, the conventional problem for the image force [28] and for a hydrophobic particle near the oil–water interface [21]. Experimentally, the nonpenetration of the field into water is manifested as independence of the configuration of the adsorbed particles on the electrolyte concentration in the aqueous phase [6,8]. Thus, in first approximation, the role of the water is to keep the electric potential constant at the boundaries S_{nw} and S_{pw} (Fig. 2). Because the latter constant can be set zero, we obtain the following two boundary conditions [8]:

$$\varphi_n = 0 \quad \text{at } S_{nw} \quad \text{and} \quad \varphi_p = 0 \quad \text{at } S_{pw}. \tag{2.2}$$

At the third interface, S_{pn}, we impose the standard boundary conditions for continuity of the electric potential and the relation between the normal electric-field components [28],

$$\varphi_n = \varphi_p \quad \text{and} \quad \mathbf{n} \cdot (\varepsilon_p \nabla \varphi_p - \varepsilon_n \nabla \varphi_n) = 4\pi \sigma_{pn} \quad \text{at } S_{pn}, \tag{2.3}$$

where ∇ is the gradient operator and $\mathbf{n}$ is the outer unit normal to the particle surface, S_{pn}.

2.2. Curvilinear coordinates

In Ref. [8] the problem (2.1)–(2.3) was solved numerically with the help of modified toroidal coordinates. Because our purpose here is to obtain analytical solution, it is more convenient to use the conventional toroidal coordinates, ξ and η, defined as follows [29–31]:

$$r = \frac{r_c}{h} \sinh \eta, \qquad z = \frac{r_c}{h} \sin \xi, \quad \text{and}$$
$$h \equiv \cosh \eta - \cos \xi. \tag{2.4}$$

Here h is a metric coefficient. The Lamé coefficients of the toroidal coordinate system, h_ξ, h_η, and h_ϕ, are [29–31]

$$h_\xi = h_\eta = \frac{r_c}{h}, \qquad h_\phi = \frac{r_c}{h} \sinh \eta. \tag{2.5}$$

The position of the contact line is determined by the pole A_+ ($\eta \to +\infty$); see Fig. 3. The axis of revolution corresponds to $\eta = 0$; the interfaces S_{nw}, S_{pn}, and S_{pw} (Fig. 2) have equations $\xi = 0$, $\xi = \xi_c$, and $\xi = \pi + \xi_c$, respectively (Fig. 3). Here, ξ_c is simply related to the angle α: $\xi_c = \pi - \alpha$. The coordinate surfaces of constant η are toroids obtained by rotation of the circumference [29–31]:

$$(r - r_c \coth \eta)^2 + z^2 = \frac{r_c^2}{\sinh^2 \eta}. \tag{2.6}$$

Likewise, the coordinate surfaces of constant ξ are spheres obtained by rotation of the circumference [29–31]:

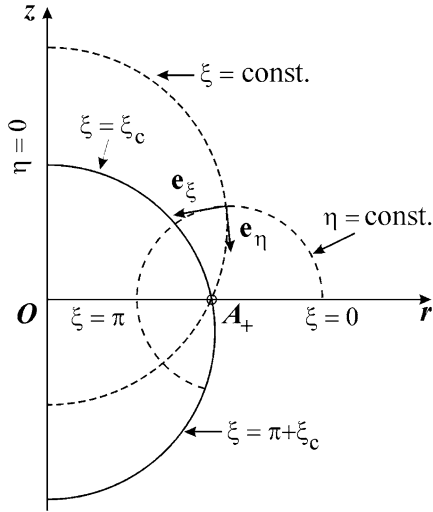$$r^2 + (z - r_c \cot \xi)^2 = \frac{r_c^2}{\sin^2 \xi}. \tag{2.7}$$

Fig. 3. Introduction of toroidal coordinates (ξ, η). The position of the contact line coincides with the pole, A_+; the interfaces S_{nw}, S_{pn}, and S_{pw} correspond to the coordinate surfaces $\xi = 0$, $\xi = \xi_c$, and $\xi = \pi + \xi_c$, respectively, where $\xi_c \equiv \pi - \alpha$ (see Fig. 2).

It is convenient to introduce dimensionless electric potentials, Φ_n and Φ_p:

$$\varphi_k = \frac{4\pi}{\varepsilon_n} r_c \sigma_{pn} \Phi_k \quad (k = n, p). \tag{2.8}$$

In view of the axial symmetry of the system, in toroidal coordinates Eq. (2.1) acquires the form [29]

$$\frac{\partial}{\partial \xi}\left(\frac{\sinh \eta}{h}\frac{\partial \Phi_k}{\partial \xi}\right) + \frac{\partial}{\partial \eta}\left(\frac{\sinh \eta}{h}\frac{\partial \Phi_k}{\partial \eta}\right) = 0 \quad \text{in } \Omega_k$$
$$(k = n, p). \tag{2.9}$$

Correspondingly, the boundary conditions, Eqs. (2.2) and (2.3), become

$$\Phi_n = 0 \quad \text{at } \xi = 0 \quad \text{and} \quad \Phi_p = 0 \quad \text{at } \xi = \pi + \xi_c, \tag{2.10}$$

$$\Phi_n = \Phi_p \quad \text{and} \quad \frac{\partial \Phi_n}{\partial \xi} - \varepsilon_{pn}\frac{\partial \Phi_p}{\partial \xi} = \frac{1}{h} \quad \text{at } \xi = \xi_c. \tag{2.11}$$

Here, as usual, $\varepsilon_{pn} = \varepsilon_p/\varepsilon_n$. The electric field intensity in the nonpolar fluid is $\mathbf{E} = -\nabla\varphi_n$. From Eq. (2.10), it follows that the tangential component of $\mathbf{E}$ at the flat interface, S_{nw}, is zero, while the normal component is

$$E_z = -\frac{4\pi}{\varepsilon_n}\sigma_{pn}(\cosh\eta - 1)\frac{\partial \Phi_n}{\partial \xi} \quad \text{at } \xi = 0, \tag{2.12}$$

where we have substituted φ_n from Eq. (2.8) and h_ξ from Eq. (2.5). As established in Ref. [8], the electrodipping force, $F^{(n)}$, exerted on the particle can be expressed as an integral of E_z^2:

$$F^{(n)} \approx \frac{4\pi}{\varepsilon_n} r_c^2 \sigma_{pn}^2 f_{\sigma\sigma},$$

$$f_{\sigma\sigma}(\alpha, \varepsilon_{pn}) = \pi \int_0^\infty \left(\frac{\partial \Phi_n}{\partial \xi}\right)_{\xi=0}^2 \sinh\eta\, d\eta \tag{2.13}$$

(see Eqs. (5.14), (5.18), and (5.19) in Ref. [8]); $F^{(n)}$ is directed toward the water phase. The integration in Eq. (2.13) is equivalent to integration of the electric pressure, p_{el}, throughout the oil–water interface; see Eq. (3.24).

3. Solution by integral transform

3.1. Application of the Mehler–Fock transform

To separate the variables in Eq. (2.9), we first replace Φ_k by a new dependent variable, Ψ_k [30–32]:

$$\Phi_k \equiv h^{1/2}\Psi_k \quad (k = n, p). \tag{3.1}$$

Then, Eq. (2.9) acquires the form [30–32]

$$L[\Psi_k] + \frac{\partial^2 \Psi_k}{\partial \xi^2} = 0 \quad \text{in } \Omega_k \quad (k = n, p), \tag{3.2}$$

where the linear differential operator, $L[\Psi]$, is

$$L[\Psi] \equiv \frac{1}{\sinh\eta}\frac{\partial}{\partial \eta}\left(\sinh\eta\frac{\partial \Psi}{\partial \eta}\right) + \frac{\Psi}{4}. \tag{3.3}$$

A substitution $u = \cosh\eta$ transforms the operator $L[\Psi]$ into the known Legendre operator:

$$L[\Psi] = \frac{\partial}{\partial u}\left[(u^2 - 1)\frac{\partial \Psi}{\partial u}\right] + \frac{\Psi}{4}. \tag{3.4}$$

The form of the operator $L[\Psi]$ suggests that the solution of Eq. (3.2) can be found by means of the Mehler–Fock integral transform [32–38]:

$$\Psi(u) = \int_0^\infty P_{-1/2+i\tau}(u)B(\tau)\, d\tau \quad (1 \leqslant u \leqslant \infty), \tag{3.5}$$

$$B(\tau) = \tau \tanh(\pi\tau)\int_1^\infty P_{-1/2+i\tau}(u)\Psi(u)\, du. \tag{3.6}$$

Equations (3.5) and (3.6) represent the forward and inverse transformations. Correspondingly, $\Psi(u)$ and $B(\tau)$ represent the original and image functions. $P_{-1/2+i\tau}(u)$ is the Legendre function of the first kind [39–41]. Here, we are dealing with Legendre function of complex index, $-1/2 + i\tau$ (τ is real; i is the imaginary unit), that could be expressed by means of the following real integral [32,42]:

$$P_{-1/2+i\tau}(\cosh\eta) = \frac{2^{1/2}}{\pi}\coth(\pi\tau)\int_\eta^\infty \frac{\sin(\tau y)\, dy}{(\cosh y - \cosh\eta)^{1/2}}. \tag{3.7}$$

The Mehler–Fock transform [32–38], and the generalized Mehler–Fock transform [38,43–45] have found applications for solving various problems of similar geometry [42,46,47]. In view of Eq. (3.5), we will seek the unknown function in the form

$$\Psi_k(\xi, \eta) = \int_0^\infty B_k(\xi, \tau)K(\eta, \tau)\, d\tau \quad (k = n, p), \tag{3.8}$$

where

$$K(\eta, \tau) \equiv P_{-1/2+i\tau}(\cosh \eta). \tag{3.9}$$

The kernel of the integral transform, $K(\eta, \tau)$, obeys the equation

$$L[K(\eta, \tau)] = -\tau^2 K(\eta, \tau). \tag{3.10}$$

The substitution of Eq. (3.8) into Eq. (3.2) yields

$$\frac{\partial^2 B_k}{\partial \xi^2} = \tau^2 B_k \quad \text{in } \Omega_k \quad (k = \text{n}, \text{p}). \tag{3.11}$$

The solution of Eq. (3.11), satisfying the boundary condition, Eq. (2.10), and $\Psi_\text{n} = \Psi_\text{p}$ at $\xi = \xi_\text{c}$, reads

$$B_\text{n}(\xi, \tau) = \Psi_\text{s}(\tau) \frac{\sinh(\xi\tau)}{\sinh(\xi_\text{c}\tau)},$$

$$B_\text{p}(\xi, \tau) = \Psi_\text{s}(\tau) \frac{\sinh[(\pi + \xi_\text{c} - \xi)\tau]}{\sinh(\pi\tau)}, \tag{3.12}$$

where $\Psi_\text{s}(\tau)$ is the image of the dimensionless electric potential at the particle–nonpolar fluid boundary.

To determine $\Psi_\text{s}(\tau)$, we first apply Eq. (3.1) to represent Eq. (2.11) in the form

$$\frac{\partial \Psi_\text{n}}{\partial \xi} - \varepsilon_\text{pn} \frac{\partial \Psi_\text{p}}{\partial \xi} + \frac{\sin \xi_\text{c}}{2h}(\Psi_\text{n} - \varepsilon_\text{pn} \Psi_\text{p}) = h_\text{c}^{-3/2}$$

$$\text{at } \xi = \xi_\text{c}. \tag{3.13}$$

Here, we have $h_\text{c} \equiv \cosh \eta - \cos \xi_\text{c}$. On the other hand, the Lebedev formula [48] yields

$$(\cosh \eta - \cos \xi_\text{c})^{-1/2} = 2^{1/2} \int_0^\infty \frac{\cosh[(\pi - \xi_\text{c})\tau]}{\cosh(\pi\tau)} K(\eta, \tau)\, d\tau. \tag{3.14}$$

The differentiation of Eq. (3.14) with respect to ξ_c yields

$$h_\text{c}^{-3/2} = \frac{2^{3/2}}{\sin \xi_\text{c}} \int_0^\infty \tau \frac{\sinh[(\pi - \xi_\text{c})\tau]}{\cosh(\pi\tau)} K(\eta, \tau)\, d\tau. \tag{3.15}$$

In view of Eqs. (3.8), (3.12), and (3.14), one can bring Eq. (3.13) into the form of an integral equation for $\Psi_\text{s}(\tau)$:

$$\int_0^\infty \Big\{ [\coth(\xi_\text{c}\tau) + \varepsilon_\text{pn} \coth(\pi\tau)] \Psi_\text{s}(\tau)$$

$$- \frac{2^{3/2}}{\sin \xi_\text{c}} \frac{\sinh[(\pi - \xi_\text{c})\tau]}{\cosh(\pi\tau)} \Big\} \tau K(\eta, \tau)\, d\tau$$

$$= -\frac{1}{2}(1 - \varepsilon_\text{pn}) \frac{\sin \xi_\text{c}}{\cosh \eta - \cos \xi_\text{c}} \int_0^\infty \Psi_\text{s}(\tau) K(\eta, \tau)\, d\tau. \tag{3.16}$$

In Section 5.1 we will demonstrate that Eq. (3.16) can be transformed into the standard form of a Fredholm integral equation of the second kind, which has a convenient numerical solution for $\Psi_\text{s}(\tau)$. The respective numerical procedure is much faster than the procedure for solving the partial differential equations in Ref. [8]. In addition, Eq. (3.16) enables one to derive useful

asymptotic expressions for the behavior of the physical variables near the contact line and far from it. Finally, for $\varepsilon_\text{pn} = 1$, Eq. (3.16) has a closed analytical solution for $\Psi_\text{s}(\tau)$, which is described in Section 4.

3.2. Expressions for the physical quantities

Having once determined $\Psi_\text{s}(\tau)$, we can further determine the electric field inside the particle and in the nonpolar fluid, by using Eqs. (3.8) and (3.12). In particular, the electric field at the boundary S_nw (at $z = 0$, see Fig. 2) can be presented in the form

$$E_z|_{z=0} = -\frac{4\pi}{\varepsilon_\text{n}} \sigma_\text{pn}(\cosh \eta - 1)^{3/2} I,$$

$$I \equiv \int_0^\infty \frac{\tau \Psi_\text{s}(\tau)}{\sinh(\xi_\text{c}\tau)} K(\eta, \tau)\, d\tau. \tag{3.17}$$

In general, $I = I(\eta, \alpha, \varepsilon_\text{pn})$. Combining Eqs. (2.13) and (3.17) we derive the following expression for the force coefficient:

$$f_{\sigma\sigma} = \frac{\pi}{2} \int_0^\infty I^2\, d[\cosh \eta - 1]^2. \tag{3.18}$$

The flat interface S_nw corresponds to the domain $r_\text{c} < r < \infty$ or, respectively, $\infty > \eta > 0$. In the calculations it is convenient to introduce the new variable x_1, which has a finite domain of variation:

$$x_1 \equiv \frac{r_\text{c}}{r} = \frac{\cosh \eta - 1}{\sinh \eta} \quad (0 < x_1 < 1). \tag{3.19}$$

From the latter expression one derives

$$\cosh \eta - 1 = \frac{2x_1^2}{1 - x_1^2}. \tag{3.20}$$

In terms of x_1, Eq. (1.4) acquires the form

$$p_\text{el}(x_1) = \frac{A_1}{r_\text{c}^6} \frac{x_1^6}{(1 - x_1)^{1-\mu}}. \tag{3.21}$$

Because $p_\text{el} \propto E_z^2|_{z=0}$, we will seek $E_z|_{z=0}$, in the form

$$E_z|_{z=0} = -\frac{4\pi \sigma_\text{pn}}{\varepsilon_\text{n}} \frac{x_1^3}{(1 - x_1)^{1-\nu}} J(x_1, \alpha, \varepsilon_\text{pn}), \tag{3.22}$$

where $2(1 - \nu) = 1 - \mu$, that is, $\nu = (1 + \mu)/2$; J is expected to be a function of bounded variation (almost constant). Note that for $x_1 \to 1$, we have $J \to C = \text{constant} \neq 0$; see Eq. (5.18). The combination of Eqs. (3.17), (3.20), and (3.22) yields

$$J(x_1, \alpha, \varepsilon_\text{pn}) \equiv \frac{2^{3/2} I(\eta, \alpha, \varepsilon_\text{pn})}{(1 + x_1)^{3/2}(1 - x_1)^{1/2+\nu}}, \tag{3.23}$$

where I is defined by Eq. (3.17), with $\Psi_\text{s}(\tau)$ being the solution of Eq. (3.16). In terms of J, the electric pressure, p_el, can be expressed in the form

$$p_\text{el}(x_1) \equiv -\frac{\varepsilon_\text{n}}{8\pi} E_z^2\big|_{z=0}$$

$$= -\frac{2\pi \sigma_\text{pn}^2}{\varepsilon_\text{n}} \frac{x_1^6}{(1 - x_1)^{2-2\nu}} [J(x_1, \alpha, \varepsilon_\text{pn})]^2. \tag{3.24}$$

In Section 5, we consider the general solution of Eq. (3.16), while in Section 4 we obtain and discuss the analytical solution to the problem in the special case $\varepsilon_p = \varepsilon_n$. The reader, who is interested in the predictions of the theory about the electrostatic force between two adsorbed particles, could go directly to Section 6.

4. Analytical solution to the problem for $\varepsilon_p = \varepsilon_n$

Examples for particle and nonpolar liquid that have equal dielectric constants are (i) glass and isopropyl ether with $\varepsilon_p \approx \varepsilon_n \approx 3.9$ and (ii) polystyrol and hexadecane with $\varepsilon_p \approx \varepsilon_n \approx 2.0$. Many solid plastics and organic liquids have close dielectric constants.

4.1. Solution of the integral equation

When the particle has the same dielectric constant as the nonpolar fluid, i.e., $\varepsilon_{pn} \equiv \varepsilon_p/\varepsilon_n = 1$, then Eq. (3.16) has an analytical solution

$$\Psi_s(\tau) = \frac{2^{3/2}}{\sin\xi_c}\sinh(\xi_c\tau)\tanh(\pi\tau)\frac{\sinh[(\pi-\xi_c)\tau]}{\sinh[(\pi+\xi_c)\tau]}. \quad (4.1)$$

The substitution of Eq. (4.1) into Eq. (3.17), along with the identity $\xi_c = \pi - \alpha$, leads to the following expression for the integral I:

$$I_e(\eta,\alpha) \equiv I(\eta,\alpha,1)$$
$$= \frac{2^{3/2}}{\sin\alpha}\int_0^\infty\frac{\tanh(\pi\tau)\sinh(\alpha\tau)}{\sinh[(2\pi-\alpha)\tau]}K(\eta,\tau)\tau\,d\tau. \quad (4.2)$$

Here and hereafter, the subscript e means that the respective quantity is estimated at equal ε_p and ε_n. The integral in Eq. (4.2) has to be solved numerically. In view of Eq. (3.9), $K(\eta,\tau)$ is related to the Legendre function, whose computation is time consuming. To speed up the numerical procedure, in Eq. (4.2) we substituted the integral expression for $P_{-1/2+i\tau}$, Eq. (3.7), and carried out the integration with respect to τ. The result reads (see Appendix B)

$$I_e = \frac{2^{3/2}\nu_e\sin(2\nu_e\xi_c)}{(\pi+\xi_c)\sin\alpha}$$
$$\times\int_0^\infty\frac{[\sinh(x)\sinh(x+\eta)]^{-1/2}\sinh[\nu_e(2x+\eta)]}{\{\cosh[\nu_e(2x+\eta)]-\cos(2\nu_e\xi_c)\}^2}\,dx, \quad (4.3)$$

where

$$\nu_e \equiv \frac{\pi}{\pi+\xi_c} = \frac{\pi}{2\pi-\alpha}. \quad (4.4)$$

The integral in Eq. (4.3) converges well because at $x \to \infty$ the integrand decays exponentially, while at $x \to 0$ it behaves as $x^{-1/2}$. A useful application of the analytical expression, Eq. (4.3), is for testing of the complicated general numerical procedure; see Section 5 and Appendix C.
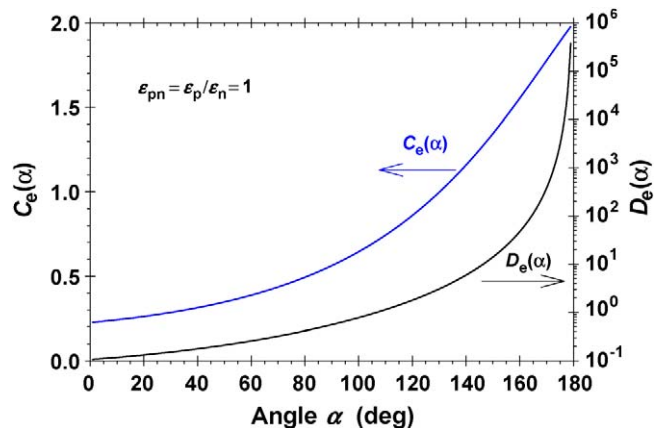

Fig. 4. Plot of D_e and C_e vs α calculated by means of Eqs. (4.6) and (4.12); $\varepsilon_{pn} = 1$.

4.2. Asymptotics of the electric field far from the particle

Far from the particle ($r \gg r_c$), we have $x_1 \to 0$ and $\eta \to 0$. In this limit, Eq. (3.22) acquires the form

$$E_z \approx -\frac{4\pi\sigma_{pn}}{\varepsilon_n}x_1^3 D_e(\alpha)\quad(z=0,\ r\gg r_c;\ \varepsilon_{pn}=1). \quad (4.5)$$

In view of Eqs. (3.23) and (4.2), we have introduced the notation

$$D_e(\alpha) \equiv J(0,\alpha,1) = 2^{3/2}I_e(0,\alpha)$$
$$= \frac{8}{\sin\alpha}\int_0^\infty\frac{\tanh(\pi\tau)\sinh(\alpha\tau)}{\sinh[(2\pi-\alpha)\tau]}\tau\,d\tau. \quad (4.6)$$

At the last step we have used the fact that $K(0,\tau) = P_{-1/2+i\tau}(1) = 1$. $D_e(\alpha)$ tends to a nonzero constant (Fig. 4), and then asymptotically $E_z \propto x_1^3$; see Eq. (4.5). Because $x_1 = r_c/r$, we have $E_z \propto r^{-3}$ for $r \gg r_c$, i.e., the electric field created by the particle at long distances behaves as the electric field of a dipole. The function $D_e(\alpha)$ determines the dependence of the effective dipole moment on the angle α. We calculated $D_e(\alpha)$ by solving numerically the integral in Eq. (4.6). The results are tabulated (Table 1 in Appendix D, the column for $\varepsilon_{pn} = 1$). The computed plot of D_e vs α is shown in Fig. 4. For $\alpha \to 0$ we have $D_e \to 1/(3\pi) = 0.1061$; see Eq. (A.11) in Appendix A.

We should also note that the right-hand side of Eq. (4.5) represents the leading term of a series expansion for $x_1 \ll 1$. It can be proven that the first neglected term in this expansion is proportional to x_1^5.

4.3. Asymptotics of the electric field near the particle

Near the contact line on the particle surface ($r \to r_c$), we have $x_1 \to 1$ and $\eta \to +\infty$. In this limit, the integral in Eq. (4.3) has the following asymptotic form:

$$I_e \approx \frac{2^{5/2}\nu_e}{\pi+\xi_c}\frac{\sin(2\nu_e\xi_c)}{\sin\alpha}\exp[-(\nu_e+0.5)\eta]$$
$$\times\int_0^\infty\frac{\exp(-2\nu_e x)}{[\exp(2x)-1]^{1/2}}\,d(2x). \quad (4.7)$$

The last integral can be taken analytically [49]. Thus we obtain

$$I_e \approx 2^{5/2} \nu_e \frac{\sin(2\nu_e \xi_c)}{\pi^{1/2} \sin \alpha} \frac{\Gamma(\nu_e + 0.5)}{\Gamma(\nu_e)} \exp\left[-(\nu_e + 0.5)\eta\right], \quad (4.8)$$

where Γ is the known gamma function [29,39–41]. From Eq. (3.14) we deduce

$$\exp(-\eta) = \frac{1 - x_1}{1 + x_1} \quad (0 < x_1 < 1). \quad (4.9)$$

Using Eq. (4.9), we obtain the form of Eq. (4.8) for $x_1 \to 1$:

$$I_e \approx 2^{2-\nu_e} \nu_e \frac{\sin(2\nu_e \xi_c)}{\pi^{1/2} \sin \alpha} \frac{\Gamma(\nu_e + 0.5)}{\Gamma(\nu_e)} (1 - x_1)^{\nu_e + 0.5}. \quad (4.10)$$

In view of Eq. (4.10), the asymptotic form of Eqs. (3.22) and (3.23) near the contact line is

$$E_z|_{z=0} = -\frac{4\pi \sigma_{pn}}{\varepsilon_n} \frac{C_e(\alpha)}{(1 - x_1)^{1-\nu_e}} \quad (x_1 \to 1), \quad (4.11)$$

$$C_e(\alpha) \equiv J(1, \alpha, 1) = \frac{2^{2-\nu_e} \pi^{1/2}}{2\pi - \alpha} \frac{\sin(\nu_e \alpha)}{\sin \alpha} \frac{\Gamma(\nu_e + 0.5)}{\Gamma(\nu_e)}. \quad (4.12)$$

The function $C_e(\alpha)$ is plotted in Fig. 4 and tabulated (Table 2 in Appendix D, the column for $\varepsilon_{pn} = 1$). For $\alpha \to 0$ we have $C_e \to 1/(2^{1/2}\pi) = 0.2251$; see Eq. (A.13) in Appendix A.

Because $0 < \alpha < \pi$, Eq. (4.4) yields $0.5 < \nu_e < 1$. Then, in view of Eq. (4.11), $E_z|_{z=0}$ has an integrable divergence for $x_1 \to 1$. On the other hand, the integral for the force coefficient, $f_{\sigma\sigma}$, is convergent. To check that, we substitute Eq. (3.20) into Eq. (3.18):

$$f_{\sigma\sigma} = 8\pi \int_1^\infty I^2 \frac{x_1^3 \, dx_1}{(1 - x_1^2)^3}. \quad (4.13)$$

For $\varepsilon_{pn} = 1$, $I = I_e$ is to be substituted from Eq. (4.10). Then, the integrand in Eq. (4.13) is $\propto (1 - x_1)^{2\nu_e - 2}$. Because $\nu_e > 0.5$, we have $2\nu_e - 2 > -1$; in other words, the integral in Eq. (4.13) is convergent. Note that such type of integrable singularities at edge-lines are typical for problems related to the calculation of the electric field in wedge shaped (angular) spatial domains; see, e.g., Ref. [28]. In our case, the wedge is formed between the surfaces S_{pn} and S_{nw}, which intersect at the contact line, $r = r_c$ (Fig. 2).

4.4. Numerical results and discussion

Equations (3.22) and (3.24) indicate that we could calculate the electric field, $E_z|_{z=0}$, and of the electric pressure, $p_{el}(x_1)$, if the function $J(x_1, \alpha, \varepsilon_{pn})$ is known. In the considered special case, $\varepsilon_{pn} = 1$, Eq. (3.23) acquires the form

$$J_e(x_1, \alpha) \equiv J(x_1, \alpha, 1) = \frac{2^{3/2} I_e(\eta, \alpha)}{(1 + x_1)^{3/2} (1 - x_1)^{1/2 + \nu_e}}, \quad (4.14)$$

where I_e and ν_e are given by Eqs. (4.3) and (4.4). Equation (3.21), which is a version of a semiempirical formula proposed in Ref. [8], assumes that $A_1 \propto J^2$ is independent of x_1; see Eq. (3.24). With the help of Eq. (4.14) we could check whether this assumption is close to the reality.
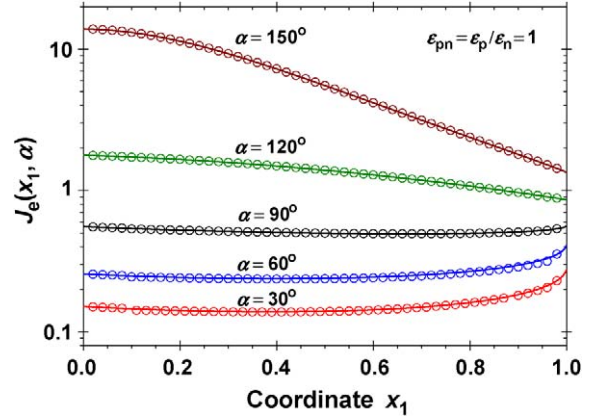

Fig. 5. Plots of J_e vs x_1 for different values of α denoted in the figure. The continuous lines are calculated from Eqs. (4.3) and (4.14). The circles are computed independently, by numerical solution of the original system partial differential equations; see Section 5.2 in Ref. [8].
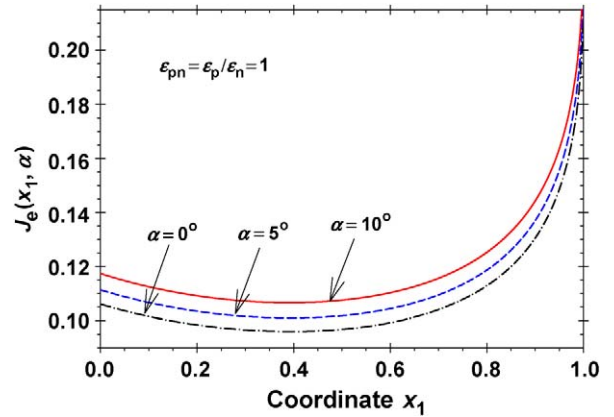

Fig. 6. Plots of J_e vs x_1 for smaller values of α denoted in the figure (cf. Fig. 4). The curves for $\alpha = 5°$ and $10°$ are calculated from Eqs. (4.3) and (4.14). The curve for $\alpha = 0$ is computed by means of Eq. (A.14) in Appendix A.

In Fig. 5 we have plotted J_e vs x_1 for several values of α. One sees that J_e is practically independent of x_1 only for $\alpha \approx 90°$. On the other hand, for $\alpha \approx 150°$ J_e varies by one order of magnitude. The accurate calculation of $E_z|_{z=0}$ and $p_{el}(x_1)$ demands J_e to be accurately calculated. The continuous lines in Fig. 5 are obtained from Eq. (4.14) by means of numerical integration of Eq. (4.3). The points denoted by circles in Fig. 5 are calculated independently, by means of the alternative procedure for solution of partial differential equations described in Section 5.2 of Ref. [8]. The excellent agreement between the two independent solutions confirms the accuracy of the used numerical procedures.

Fig. 6 shows plots of J_e vs x_1 again, but this time for smaller values α, viz. $\alpha = 0°$, $5°$, and $10°$. The curve for $\alpha = 0$ is drawn by means of the analytical expression derived in Appendix A; see Eq. (A.14) therein. One sees that the curves in Fig. 6 vary between 0.1 and 0.215, i.e., the magnitude of J_e could change about two times.

Plot of the force coefficient $f_{\sigma\sigma}$ vs α is shown in Fig. 7 for $\varepsilon_{pn} = 1$. $f_{\sigma\sigma}$ is calculated from Eq. (4.13), where $I = I_e$ is obtained from Eq. (4.3). In both Eqs. (4.13) and (4.3) the inte-
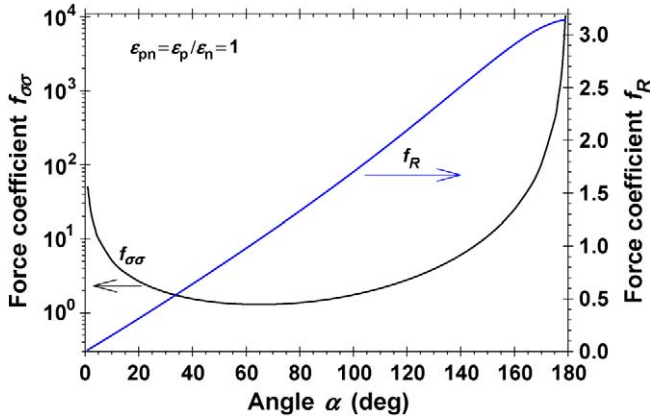
Fig. 7. Dependence of the force coefficients $f_{\sigma\sigma}$ and $f_R \equiv f_{\sigma\sigma}\sin^2\alpha$ on α for $\varepsilon_{\mathrm{pn}} = 1$. The curves are calculated with the help of Eqs. (4.3) and (4.13).

gration is carried out numerically. As seen in Fig. 7, $f_{\sigma\sigma}$ varies by orders of magnitude as a function of α, and has a minimum at $\alpha \approx 65°$. In addition, $f_{\sigma\sigma}$ exhibits a logarithmic divergence at $\alpha \to 0$; see Appendix A. The latter facts indicate that $f_{\sigma\sigma}$ is not a convenient parameter, from both computational and physical viewpoint. To find a more convenient force coefficient, we considered the following three equivalent expressions for the electrodipping force:

$$
\begin{aligned}
F^{(\mathrm{n})} &= \frac{4\pi}{\varepsilon_{\mathrm{n}}}\sigma_{\mathrm{pn}}^2 R^2 (1-\cos\alpha) f(\alpha, \varepsilon_{\mathrm{pn}}) \\
&= \frac{4\pi}{\varepsilon_{\mathrm{n}}}\sigma_{\mathrm{pn}}^2 r_{\mathrm{c}}^2 f_{\sigma\sigma}(\alpha, \varepsilon_{\mathrm{pn}}) \\
&= \frac{4\pi}{\varepsilon_{\mathrm{n}}}\sigma_{\mathrm{pn}}^2 R^2 f_R(\alpha, \varepsilon_{\mathrm{pn}}).
\end{aligned}
\tag{4.15}
$$

The coefficient $f(\alpha, \varepsilon_{\mathrm{pn}})$ was computed and tabulated in [8], see Eq. (1.2); the coefficient $f_{\sigma\sigma}(\alpha, \varepsilon_{\mathrm{pn}})$ was also used in the theoretical derivations therein. The coefficient $f_R \equiv f_{\sigma\sigma}\sin^2\alpha$ is plotted vs α in Fig. 7 for $\varepsilon_{\mathrm{pn}} = 1$. One sees that f_R exhibits a simple monotonic dependence on α, and that f_R is regular in the whole interval $0 \leqslant \alpha \leqslant \pi$, where $0 \leqslant f_R \leqslant \pi$. The greatest value, $f_R(\alpha = \pi) = \pi$, corresponds to a spherical particle into oil, that has only a point contact with the water; the same limiting value is obtained independently in Ref. [21].

Physically, the increase of f_R with α (Fig. 7) corresponds to the fact that for a particle of fixed radius, R, with the rise of α, the area of the electrically charged interface S_{pn}, increases (Fig. 2). For greater charge at S_{pn}, the electrodipping force, $F^{(\mathrm{n})}$, and the respective force coefficient, f_R, must be also greater.

The transparent physical meaning of $f_R(\alpha)$, and its regular behavior (Fig. 7), make f_R the most convenient force coefficient. For this reason, in Table 3 of Appendix D we have tabulated the dependence $f_R(\alpha, \varepsilon_{\mathrm{pn}})$ for the needs of a fast and convenient calculation of the electrodipping force $F^{(\mathrm{n})}$. For $\varepsilon_{\mathrm{pn}} = 1$, f_R is computed by integration in Eqs. (4.13) and (4.3). The columns with $\varepsilon_{\mathrm{pn}} \neq 1$ are computed with the help of the general theory in Section 5.

5. Solution to the general problem for $\varepsilon_{\mathrm{p}} \neq \varepsilon_{\mathrm{n}}$

In the general case when $\varepsilon_{\mathrm{p}} \neq \varepsilon_{\mathrm{n}}$, we cannot find a simple analytical solution of Eq. (3.16) for $\Psi_{\mathrm{s}}(\tau)$, like Eq. (4.1). Nevertheless, in this case Eq. (3.16) can be solved by using a convenient and accurate procedure that is described in Section 5.1.

5.1. Reduction of the problem to Fredholm equation

First, we subject Eq. (3.16) to the inverse Mehler–Fock transform, Eq. (3.6),

$$
\begin{aligned}
\Psi_{\mathrm{s}}(\tau) &= \frac{2^{3/2}(1-\beta)}{\sin\xi_{\mathrm{c}}}\frac{\sinh(\alpha\tau)}{\sinh(\pi\tau)}g^2(\tau) \\
&\quad + \beta\sin\xi_{\mathrm{c}}g^2(\tau)\int_0^\infty \Psi_{\mathrm{s}}(\tilde{\tau})U(\tau,\tilde{\tau})\,\mathrm{d}\tilde{\tau},
\end{aligned}
\tag{5.1}
$$

where

$$
g^2(\tau) \equiv \frac{\tanh(\pi\tau)\sinh(\pi\tau)\sinh(\xi_{\mathrm{c}}\tau)}{\sinh[(\pi+\xi_{\mathrm{c}})\tau] - \beta\sinh(\alpha\tau)}.
\tag{5.2}
$$

Here, as usual, $\xi_{\mathrm{c}} = \pi - \alpha$; the definitions of the dimensionless parameter β and the kernel U are as follows:

$$
\beta \equiv \frac{\varepsilon_{\mathrm{p}} - \varepsilon_{\mathrm{n}}}{\varepsilon_{\mathrm{p}} + \varepsilon_{\mathrm{n}}} = \frac{\varepsilon_{\mathrm{pn}} - 1}{\varepsilon_{\mathrm{pn}} + 1},
\tag{5.3}
$$

$$
U(\tau,\tilde{\tau}) \equiv \int_0^\infty \frac{K(\eta,\tau)K(\eta,\tilde{\tau})}{\cosh\eta - \cos\xi_{\mathrm{c}}}\sinh\eta\,\mathrm{d}\eta.
\tag{5.4}
$$

Note that $U(\tau,\tilde{\tau})$ is a symmetric function of its arguments. The procedure for calculation of $K(\eta,\tau)$ and $U(\tau,\tilde{\tau})$ is described in Appendix C.

Next, it is convenient to introduce two new functions, G and V, as follows:

$$
\begin{aligned}
G(\tau) &\equiv \Psi_{\mathrm{s}}(\tau)/g(\tau), \\
V(\tau,\tilde{\tau}) &\equiv \beta\sin\xi_{\mathrm{c}}g(\tau)g(\tilde{\tau})U(\tau,\tilde{\tau}).
\end{aligned}
\tag{5.5}
$$

Thus, Eq. (5.1) acquires the form of an integral equation of Fredholm of the second kind [50],

$$
G(\tau) = b(\tau) + \int_0^\infty V(\tau,\tilde{\tau})G(\tilde{\tau})\,\mathrm{d}\tilde{\tau},
\tag{5.6}
$$

where

$$
b(\tau) \equiv \frac{2^{3/2}(1-\beta)}{\sin\xi_{\mathrm{c}}}\frac{\sinh(\alpha\tau)}{\sinh(\pi\tau)}g(\tau).
\tag{5.7}
$$

One could check that the functions b^2 and V^2 are integrable over the domain $0 < \tau < \infty$. Moreover, $V(\tau,\tilde{\tau})$ is a symmetric function of its arguments. In such a case, $G(\tau)$ can be found as a solution of Eq. (5.6), by iterations [51]. To start the iterations, we substituted $G(\tilde{\tau}) = b(\tilde{\tau})$ on the right-hand side of Eq. (5.6). This simple iteration procedure converges fast. In our computations, to achieve a relative error of 10^{-8}, the maximum number of iterations was 30 for $\varepsilon_{\mathrm{pn}} = 8$.

The calculation of the kernel, V, is much more time consuming than the numerical solution of the integral equation. The computations can be accelerated in the following way. The function, U, defined by Eq. (5.4), depends on α, but it is independent of ε_{pn}. As described in Appendix C, we calculated U, and stored the dependence of U on α. The stored numerical data were further used to compute the parameters in the tables in Appendix D for various ε_{pn}.

5.2. Asymptotics of the electric field far from the particle

As mentioned in Section 4.2, far from the particle ($r \gg r_c$), we have $x_1 \to 0$ and $\eta \to 0$. In this limit, with the help of Eq. (3.20), one can bring Eq. (3.17) into the form

$$E_z|_{z=0} \approx -\frac{4\pi\sigma_{pn}}{\varepsilon_n} x_1^3 D(\alpha, \varepsilon_{pn}) \quad (r \gg r_c), \tag{5.8}$$

where

$$D(\alpha, \varepsilon_{pn}) \equiv 2^{3/2} \int_0^\infty \frac{\tau \Psi_s(\tau)}{\sinh(\xi_c \tau)}\, d\tau. \tag{5.9}$$

In Eq. (3.17), we have used the fact that $K(0, \tau) = P_{-1/2+i\tau}(1) = 1$. Note that Eqs. (4.5), (4.6) represent a special case of Eqs. (5.8), (5.9) for $\varepsilon_{pn} = 1$. Equation (5.8) expresses the leading term of a truncated series expansion, the first neglected term being of the order of x_1^5. For $x_1 \to 0$, Eq. (5.8) predicts $E_z \propto x_1^3 \propto r^{-3}$. In other words, as mentioned above, at long distances the electric field created by the particle behaves as the field of a dipole. The function $D(\alpha, \varepsilon_{pn})$ is proportional to the dipole moment; see Section 6 for details. To calculate $D(\alpha, \varepsilon_{pn})$, we first determined $\Psi_s(\tau)$ as explained in Section 5.1 and Appendix C, and then we computed numerically the integral in Eq. (5.9). The dependence $D(\alpha, \varepsilon_{pn})$ is tabulated (see Table 1 in Appendix D).

Fig. 8 shows the calculated plots of D vs α for five different values of ε_{pn}. One sees that D increases by several orders of magnitude with the rise of α. On the other hand, D decreases with the increase of ε_{pn}. The physical consequences of this behavior are discussed in Section 6, where the electrostatic interaction between two adsorbed particles is considered.

5.3. Determination of the power ν in the short-range asymptotics

In the special case $\varepsilon_{pn} = 1$, the power ν_e is expressed by Eq. (4.4). In the general case $\varepsilon_{pn} \neq 1$, such explicit expression for ν is missing. Instead, ν can be determined as the smallest positive root of Eq. (5.17); see below.

We recall that ν characterizes the integrable divergence of $E_z(x_1)$ and $p_{el}(x_1)$ for $x_1 \to 1$, i.e., at the contact line on the particle surface; see Eqs. (3.22) and (3.24). The contact line represents the edge-line of the wedge-shaped zone confined between the surfaces S_{pn} and S_{nw} near the particle. Analogous problem has been solved in Ref. [28] for a wedge with planar surfaces. Here, our problem is more complicated, because the
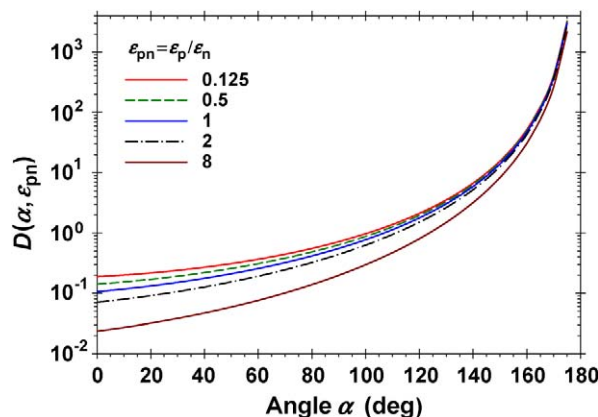

Fig. 8. Dependence of D on α for various ε_{pn} denoted in the figure. The curves are calculated with the help of Eq. (5.9).

surface S_{pn} is spherical and the edge-line is curved; therefore, we have to use curvilinear coordinates.

In view of Eq. (3.3), the asymptotic form of Eq. (3.2) for $\eta \to \infty (x_1 \to 1)$ is

$$\frac{\partial^2 \Psi_{k,0}}{\partial \eta^2} + \frac{\partial \Psi_{k,0}}{\partial \eta} + \frac{\Psi_{k,0}}{4} + \frac{\partial^2 \Psi_{k,0}}{\partial \xi^2} = 0 \quad (k = n, p). \tag{5.10}$$

Here, $\Psi_{n,0}$ and $\Psi_{p,0}$ are the leading terms in the expansions of Ψ_n and Ψ_p for $\eta \to \infty$. In the same limit, we have set $\coth \eta \approx 1$. In the frame of the same approximation, the boundary conditions, Eqs. (2.10), (2.11), and (3.13) acquire the form

$$\Psi_{n,0} = 0 \quad \text{at } \xi = 0, \qquad \Psi_{p,0} = 0 \quad \text{at } \xi = \pi + \xi_c, \tag{5.11}$$

$$\Psi_{n,0} = \Psi_{p,0} \quad \text{and} \quad \varepsilon_n \frac{\partial \Psi_{n,0}}{\partial \xi} = \varepsilon_p \frac{\partial \Psi_{p,0}}{\partial \xi} \quad \text{at } \xi = \xi_c. \tag{5.12}$$

Equations (5.10)–(5.12) define the boundary problem in the considered close vicinity of the contact line. The general solution of Eq. (5.10), that satisfies Eq. (5.11), is

$$\Psi_{n,0} = X_n \exp[-(0.5 + \nu)\eta] \sin(\nu\xi), \tag{5.13}$$

$$\Psi_{p,0} = X_p \exp[-(0.5 + \nu)\eta] \sin[\nu(\pi + \xi_c - \xi)], \tag{5.14}$$

where X_n and X_p are unknown coefficients. The substitution of Eqs. (5.13) and (5.14) into the boundary conditions, Eq. (5.12) leads to the following homogeneous system of linear equations for X_n and X_p:

$$\sin(\nu\xi_c)X_n - \sin(\nu\pi)X_p = 0,$$
$$\cos(\nu\xi_c)X_n + \varepsilon_{pn}\cos(\nu\pi)X_p = 0. \tag{5.15}$$

This system will have a nontrivial solution, when the determinant of the system is equal to zero, i.e.,

$$\varepsilon_{pn}\sin(\nu\xi_c)\cos(\nu\pi) + \cos(\nu\xi_c)\sin(\nu\pi) = 0. \tag{5.16}$$

Having in mind that $\xi_c = \pi - \alpha$, after some transformations we bring Eq. (5.16) into the form

$$\sin[(2\pi - \alpha)\nu] = \beta \sin(\alpha\nu), \tag{5.17}$$

where β is defined by Eq. (5.3). Equation (5.17) has an infinite series of positive roots $\nu_1 < \nu_2 < \nu_3 < \cdots$. For $-1 < \beta < 1$, the smallest root, ν_1, is always between 0.5 and 1.0; moreover, we always have $\nu_2 > 1$. Equation (3.22) indicates that
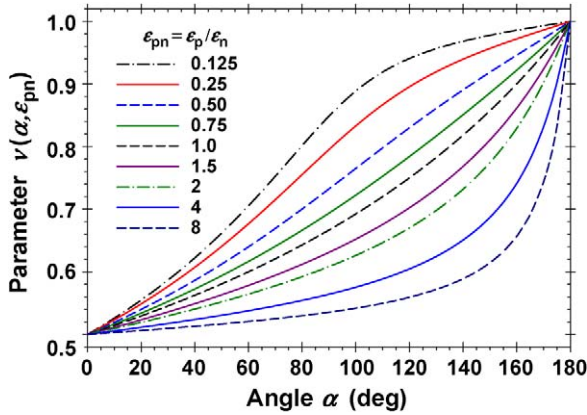
Fig. 9. Dependence of ν on α for various ε_{pn} denoted in the figure; ν is calculated as the smallest positive root of Eq. (5.17).
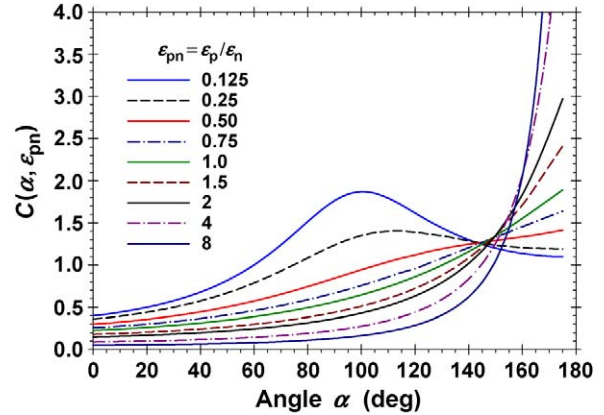

Fig. 10. Dependence of C on α for various ε_{pn} denoted in the figure. The curves are calculated as explained in the text.

$E_z|_{z=0} \propto (1 - x_1)^{\nu-1}$, and consequently, only the first root, ν_1, corresponds to singularity, whereas the other roots, $\nu_2, \nu_3, \ldots$, do not give contribution to the singularity of the electric field at the contact line. In the special case $\varepsilon_{pn} = 1$ ($\beta = 0$), Eq. (5.17) gives $\nu_1 = \nu_e$, where ν_e is given by Eq. (4.4).

As we are interested in the leading (singular) term in the expansion of $E_z|_{z=0}$ at $x_1 \to 1$, hereafter we will set $\nu \equiv \nu_1$. The dependence $\nu = \nu(\alpha, \varepsilon_{pn})$, calculated from Eq. (5.17), is tabulated in Appendix D (Table 4 therein) and illustrated in Fig. 9. As seen in this figure, the limiting values of ν are $\nu(\alpha = 0) = 0.5$ and $\nu(\alpha = \pi) = 1$ (see also Table 4 in Appendix D). The latter value, corresponding to point contact of the particle with the water phase, indicated the absence of singularity, as independently established in Ref. [21] for this special case.

In general, ν increases monotonically with the rise of both α and ε_{pn} (Fig. 9). Because $E_z|_{z=0} \propto (1 - x_1)^{\nu-1}$, the most pronounced singularity takes place at the smallest value of ν, viz., $\nu = 0.5$, which corresponds to a particle (immersed in water) that has a point contact with the nonpolar fluid (oil, air).

5.4. Asymptotics of the electric field near the particle

The limiting form of Eq. (3.22) near the contact line ($x_1 \to 1$) is

$$E_z|_{z=0} = -\frac{4\pi}{\varepsilon_n} \sigma_{pn} C (1 - x_1)^{\nu-1} \quad (x_1 \to 1), \tag{5.18}$$

where

$$C(\alpha, \varepsilon_{pn}) \equiv \lim_{x_1 \to 1} J(x_1, \alpha, \varepsilon_{pn}) \tag{5.19}$$

and where ν is the smallest positive root of Eq. (5.17). We determined $C(\alpha, \varepsilon_{pn})$ numerically, in the framework of the calculation of $J(x_1, \alpha, \varepsilon_{pn})$, which is considered in Section 5.5. For $x_1 \to 1$, the computed J tends to a constant, which is equal to C, in accordance with Eq. (5.19). Numerical results for $C(\alpha, \varepsilon_{pn})$ are tabulated in Appendix D and illustrated in Fig. 10. One sees that for the smaller ε_{pn}, the dependence $C(\alpha)$ exhibits a maximum, whereas for the greater ε_{pn} it is monotonic. For $\alpha < 145°$, C decreases with the rise of ε_{pn}, while for $\alpha > 145°$ this tendency is inverted.

To check how important is the asymptotics of E_z at $x_1 \to 1$ for the electrodipping force, we represent Eq. (4.13) in the form

$$f_{\sigma\sigma} = 8\pi \int_0^{1-\delta} \left(\frac{\varepsilon_n E_z}{4\pi \sigma_{pn}} \right)^2_{z=0} \frac{dx_1}{x_1^3}$$

$$+ 8\pi \int_{1-\delta}^1 \left(\frac{\varepsilon_n E_z}{4\pi \sigma_{pn}} \right)^2_{z=0} \frac{dx_1}{x_1^3}. \tag{5.20}$$

To obtain Eq. (5.20), we first substituted I from Eq. (3.17) into Eq. (4.13), and then replaced $\cosh \eta - 1$ from Eq. (3.20); δ is a small parameter. The second integral on the right-hand side of Eq. (5.20) can be estimated by substituting $E_z|_{z=0}$ from Eq. (5.18):

$$8\pi \int_{1-\delta}^1 \left(\frac{\varepsilon_n E_z}{4\pi \sigma_{pn}} \right)^2_{z=0} \frac{dx_1}{x_1^3} = \pi C^2 \frac{\delta^{2\nu-1}}{2\nu - 1}. \tag{5.21}$$

For $\nu \to 0.5$, the right-hand side of Eq. (5.21) could become large. For example, for $\delta = 0.001$ and $2\nu - 1 = 0.01$, we have $\delta^{2\nu-1}/(2\nu - 1) = 93.33$. This fact could lead to inaccuracies when $f_{\sigma\sigma}$ is calculated by numerical integration with a finite step. For this reason, at the smaller α, the values of the force coefficient $f(\alpha, \varepsilon_{pn})$ determined from Table 4 in Ref. [8] could differ in the frame of $\pm 15\%$ from the exact values of this quantity calculated here on the basis of the exact analytical asymptotics (see the table for f_R in Appendix D).

In fact, $\nu \to 0.5$ for $\alpha \to 0$ (see Fig. 9), which corresponds to a particle situated in water and having only a point contact with the nonpolar phase. In this limit, $f_{\sigma\sigma}$ has a logarithmic singularity (Appendix A), but the physical force coefficient, $f_R \equiv f_{\sigma\sigma} \sin^2 \alpha$, tends to zero because of the multiplier $\sin^2 \alpha$; see Eq. (4.15) and Fig. 11.

5.5. Calculation of f_R and J in the general case when $\varepsilon_{pn} \neq 1$

To calculate $f_R(\alpha, \varepsilon_{pn})$ and $J(x_1, \alpha, \varepsilon_{pn})$ in the general case $\varepsilon_{pn} \neq 1$, we first solved Eq. (5.6) and determined $\Psi_s(\tau)$, as explained in Section 5.1 and Appendix C. Then, $\Psi_s(\tau)$ was substituted in Eq. (3.17) to determine I. Next, I was substituted in
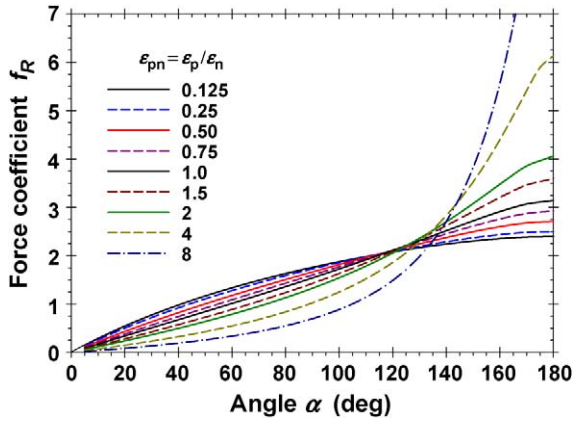
Fig. 11. Dependence of the force coefficient f_R on α for various ε_{pn} denoted in the figure. The curves are calculated as explained in Section 5.5.

(a)

(b)

Fig. 12. Plots of J vs x_1 for different values of α denoted in the figure. (a) $\varepsilon_{pn} = 0.5$; (b) $\varepsilon_{pn} = 2$. The continuous lines are calculated as explained in Section 5.5. The circles are computed independently, by numerical solution of the original system partial differential equations; see Section 5.2 in Ref. [8].

Eqs. (3.23) and (4.13) to calculate J and $f_{\sigma\sigma}$. Finally, we used the relationship $f_R \equiv f_{\sigma\sigma} \sin^2 \alpha$.

The calculated $f_R(\alpha, \varepsilon_{pn})$ is tabulated in Appendix D and illustrated in Fig. 11. As seen in the figure, f_R is monotonically increasing with the rise of α. This behavior is related to the fact that the area of the particle–nonpolar fluid interface (and the total surface charge) is larger for greater angle α. In particular, for $\alpha = 0$ this area is zero and $f_R = 0$. The dependence of f_R on ε_{pn} is more complicated. For $\alpha < 120°$, f_R grows with the rise of ε_{pn}, but for greater α this tendency is inverted (Fig. 11). f_R has no singular points in the whole interval $0 \leqslant \alpha \leqslant 180°$. For example, for $\varepsilon_{pn} = 8$, $f_R(180°) = 11.10$ (not shown in Fig. 11). For $\alpha = 180°$ it is preferable to use the theoretical expressions in Ref. [21], to avoid computational problems related to singularity in the coordinate transformation in Section 2.2. The values of $f_R(\alpha, \varepsilon_{pn})$, tabulated in Appendix D, can be used for calculation of the electrodipping force, $F^{(n)}$, with the help of Eq. (4.15). If $F^{(n)}$ is experimentally measured, the tabulated numerical data for $f_R(\alpha, \varepsilon_{pn})$ enable one to determine the surface charge density, σ_{pn}; see Ref. [8] for details.

Figs. 12a and 12b show calculated curves $J(x_1)$ for several values of α and two values of ε_{pn}. We recall that we need to know $J(x_1, \alpha, \varepsilon_{pn})$ for calculating the electric field $E_z|_{z=0}$ and the electric pressure, $p_{el}(r)$, by means of Eqs. (3.22) and (3.24). As expected, $J(x_1)$ is a function of bounded variation, which is almost constant for α about 90°. The strongest dependence of J on x_1 is observed for the more hydrophobic particles, see the curve with $\alpha = 150°$ in Fig. 12. On the other hand, J exhibits a pronounced dependence on α: J could rise by two orders of magnitude when α increases from 30° to 150°. The comparison between Figs. 12a and 12b indicates that the increase of ε_{pn} produces some effect on J, but this effect is much weaker than the influence of α.

As in Fig. 5, the continuous lines in Fig. 12 are obtained by using the equations derived in the present paper, whereas the points denoted by circles are calculated independently, by means of the procedure for solution of partial differential equations described in Section 5.2 of Ref. [8]. It should be noted that the density of the integration grid used in Ref. [8] is greater than the density of the points (the circles) shown in Figs. 5 and 12.
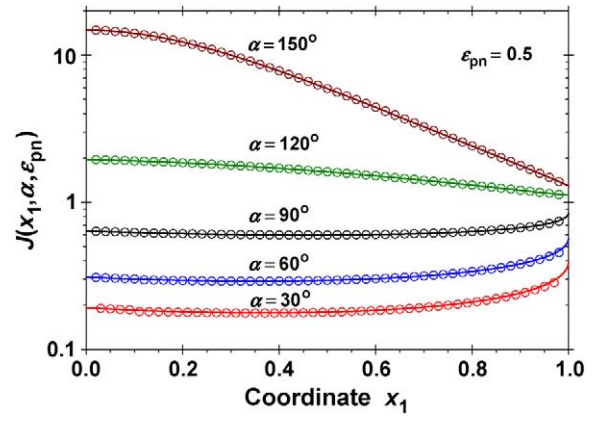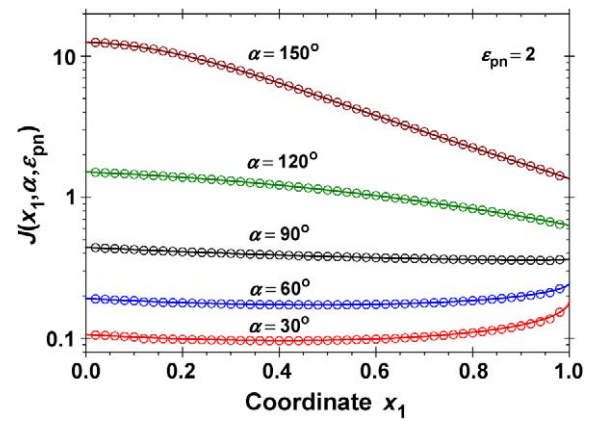
(We had to decrease the density of the circles shown in the figures to make the continuous line visible.) In both Figs. 5 and 12, the agreement between the two independent solutions is excellent and confirms the accuracy of the two different computational procedures.

6. Asymptotic expression for the lateral electric force between two particles

Here, we consider two particles which are attached to the water–nonpolar fluid boundary, and which are separated at a center-to-center distance L (Fig. 13). In accordance with Eq. (5.8), for $r \gg r_c$ the electric field generated by each particle in isolation is identical to the electric field of a dipole, whose dipole moment is perpendicular to the water–nonpolar fluid interface,

$$E_x|_{z=0} = 0, \quad E_z|_{z=0} \approx -\frac{p_d}{\varepsilon_n r^3} \quad (r \gg r_c), \tag{6.1}$$

where the effective dipole moment is

$$p_d = 4\pi \sigma_{pn} r_c^3 D = 4\pi \sigma_{pn} R^3 D \sin^3 \alpha. \tag{6.2}$$

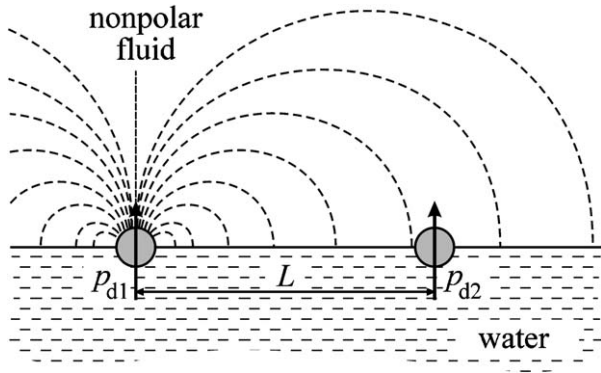$D = D(\alpha, \varepsilon_{pn})$ is defined by Eq. (5.9); it is tabulated in Appendix D and illustrated in Fig. 8.

Fig. 13. Two particles attached to the water–nonpolar fluid boundary, which are separated at a center-to-center distance L. For $L \gg r_{\rm c}$, the electric field of each particle in isolation is identical to the electric field of a dipole, whose dipole moment is given by Eq. (6.2).

Fig. 14. Plot of $D \sin^3 \alpha$ vs α for various $\varepsilon_{\rm pn}$ denoted in the figure. The dipole moment $p_{\rm d} \propto D \sin^3 \alpha$ increases monotonically with the rise of α; see Eq. (6.2). The values of D are the same as in Fig. 8.

The force of electrostatic interaction between two such particles-dipoles (Fig. 13) is

$$F_{12} = \frac{3 p_{\rm d1} p_{\rm d2}}{2 \varepsilon_{\rm n} L^4} \quad (R/L \ll 1). \tag{6.3}$$

Here, $p_{\rm d1}$ and $p_{\rm d2}$ are the dipole moments defined by Eq. (6.2), but in general, they could correspond to different particle radii, R_1 and R_2, dielectric constants, $\varepsilon_{\rm p1}$ and $\varepsilon_{\rm p2}$, contact angles, α_1 and α_2, and surface charge densities, $\sigma_{\rm pn1}$ and $\sigma_{\rm pn2}$. The factor 2 in the denominator of Eq. (6.3) accounts for the fact that the dipolar field occupies only the upper half-space (the nonpolar fluid), see Fig. 13. Indeed, as mentioned above, the electric field, created by charges in the nonpolar phases, practically does not penetrate into the water phase due to its greater dielectric constant. The presence of dissolved electrolyte in the aqueous phase additionally suppresses the penetration of electric fields from the oil into the water [21].

As indicated by Eq. (6.2), the dipole moment $p_{\rm d}$ is proportional to $D \sin^3 \alpha$. In Fig. 14 we have plotted $D \sin^3 \alpha$ vs α for various values of $\varepsilon_{\rm pn}$. One sees that $p_{\rm d} \propto D \sin^3 \alpha$ increases monotonically with the rise of α, but decreases when $\varepsilon_{\rm pn}$ increases. In particular, the divergence of D for $\alpha \to 180°$ (Fig. 8) is compensated by the fact that $\sin^3 \alpha \to 0$ in the same limit, so that $p_{\rm d}$ is finite for all $\alpha \in [0, 180°]$.

In general, the increase of $p_{\rm d} \propto D \sin^3 \alpha$ with the rise of α (Fig. 14) correlates with the experimental fact that the repulsion between adsorbed particles increases when the particles are more hydrophobic; see Ref. [6]. In the latter study, for $\alpha \geqslant 129°$ the repulsion between the particles was so strong that they formed hexagonal lattices whose constant was considerably greater than the particle diameter. On the other hand, for $\alpha \leqslant 115°$ the repulsion weakened, and the particles coagulated and formed surface aggregates [6].

In general, the interaction described by Eq. (6.3) is repulsion when $\sigma_{\rm pn1}$ and $\sigma_{\rm pn2}$ have similar signs and attraction if $\sigma_{\rm pn1}$ and $\sigma_{\rm pn2}$ have the opposite signs. The respective interaction energy is

$$U_{12} = \int_L^\infty F_{12}(\hat{L}) \, {\rm d}\hat{L} = \frac{p_{\rm d1} p_{\rm d2}}{2 \varepsilon_{\rm n} L^3} \quad (R/L \ll 1). \tag{6.4}$$
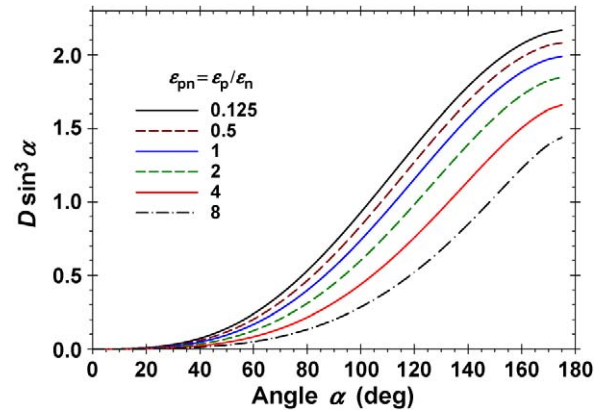
As mentioned above, the Coulombic interaction of adsorbed particles across the oily phase was experimentally established in Ref. [1] and estimated by means of the following formula [1, 6,12]:

$$U_{12} = \frac{(A_{\rm pn} \sigma_{\rm pn})^2}{\varepsilon_{\rm n} L} \left\{ 1 - \left[1 + (3 + \cos\alpha)^2 R^2/L^2 \right]^{-1/2} \right\}. \tag{6.5}$$

In Eq. (6.5) the case of two identical particles is considered; $A_{\rm pn} = 2\pi R^2 (1 - \cos\alpha)$ is the area of the particle–nonpolar fluid interface. The asymptotics of Eq. (6.5) for $R^2/L^2 \ll 1$ reads

$$U_{12} \approx \frac{[A_{\rm pn} \sigma_{\rm pn} R (3 + \cos\alpha)]^2}{2 \varepsilon_{\rm n} L^3} \quad \text{for } R^2/L^2 \ll 1. \tag{6.6}$$

The comparison of Eqs. (6.6) and (6.4) shows that the effective dipole moment in Eq. (6.6) is $p_{\rm d}^* = A_{\rm pn} \sigma_{\rm pn} R (3 + \cos\alpha)^2$. The ratio of the exact dipole moment $p_{\rm d}$ in Eq. (6.2) and the estimated dipole moment, $p_{\rm d}^*$, is

$$\frac{p_{\rm d}}{p_{\rm d}^*} = \frac{2D(\alpha, \varepsilon_{\rm pn}) \sin^3 \alpha}{(1 - \cos\alpha)(3 + \cos\alpha)}. \tag{6.7}$$

In Fig. 15 we have plotted $p_{\rm d}/p_{\rm d}^*$ vs α for various $\varepsilon_{\rm pn}$. One sees that $p_{\rm d}/p_{\rm d}^*$ is close to 1 for the greater α and smaller $\varepsilon_{\rm pn}$. In all other cases, one should use the exact Eq. (6.2), which accounts for the effect of $\varepsilon_{\rm pn}$ on $p_{\rm d}$.

7. Limits of applicability of the developed theory

The theory developed in the present paper is sufficient for quantitative description of the electrodipping force, $F^{(\rm el)}$, when the following two relations are satisfied:

$$F^{(\rm el)} \equiv F^{(\rm w)} + F^{(\rm n)} \approx F^{(\rm n)}, \tag{7.1}$$

$$F^{(\rm n)} \approx \frac{4\pi}{\varepsilon_{\rm n}} \sigma_{\rm pn}^2 r_{\rm c}^2 f_{\sigma\sigma}(\alpha, \varepsilon_{\rm pn}); \tag{7.2}$$

see Eqs. (1.1) and (4.15). Equation (7.1) means that the contribution of surface charges at the particle–water interface is much smaller than the contribution of charges at the particle–nonpolar fluid boundary, i.e., $F^{(\rm w)} \ll F^{(\rm n)}$. Experimental indication for

Fig. 15. Plot of p_d/p_d^* vs α for various ε_{pn}. The curves are calculated by means of Eq. (6.7) where D is the same as in Fig. 8.

the fulfillment of Eq. (7.1) is the independence of the particle configuration on the variation of electrolyte concentration in the aqueous phase. This was observed with particles of radius $R = 200$–300 μm in Ref. [8], but it was also detected with much smaller particles,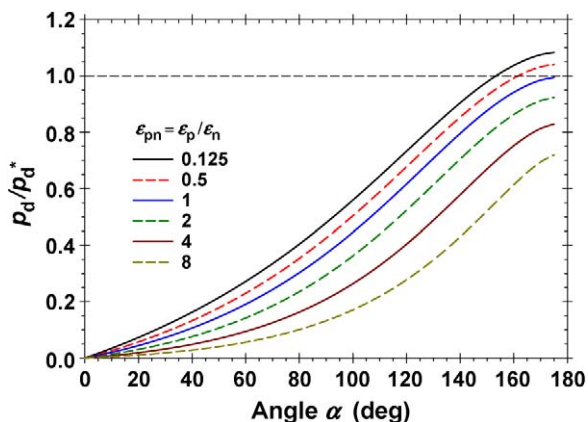 $R = 1$ μm, in Ref. [6]. On the other hand, indication about a possible effect of $F^{(w)}$ was found in [3], where the order–disorder transition in particle monolayers was sensitive to the concentration of salt in the water. In general, one could expect that the effect of $F^{(w)}$ should become significant for relatively small particles, for which the particle radius is comparable to the thickness of the adjacent electric double layer in the water.

Equation (7.2) is an approximated version of Eq. (5.14) in Ref. [8], which reads

$$F^{(n)} = \frac{4\pi}{\varepsilon_n} r_c^2 \sigma_{pn}^2 f_{\sigma\sigma} + 2r_c\sigma_{pn}(\Delta\varphi)f_{\varphi\sigma} + \frac{\varepsilon_n}{4\pi}(\Delta\varphi)^2 f_{\varphi\varphi}, \quad (7.3)$$

where $\Delta\varphi$ is the difference between the electric potentials at the particle–water and nonpolar fluid–water boundaries; the dimensionless functions $f_{\varphi\varphi}$, $f_{\varphi\sigma}$, and $f_{\sigma\sigma}$ depend on α and ε_{pn}, and all of them are of the order of 1. (Note that Eq. (2.2) is equivalent to setting $\Delta\varphi = 0$.) For typical parameter values, $r_c = 200$ μm, $\varepsilon_n = 2$, $\sigma_{pn} = 80$ μC/m² (2000 nm² per charge), and $\Delta\varphi = 60$ mV, the magnitude of the terms in Eq. (7.3) is [8]

$$F^{(n)} = [1.45f_{\sigma\sigma} + 1.92 \times 10^{-4} f_{\varphi\sigma} + 6.37 \times 10^{-9} f_{\varphi\varphi}]$$
$$\times 10^{-5} \text{ N}. \quad (7.4)$$

One sees that for $r_c = 200$ μm the terms with $f_{\varphi\sigma}$ and $f_{\varphi\varphi}$ are completely negligible and Eq. (7.3) reduces to Eq. (7.2). However, for $r_c = 20$ nm the three terms in Eq. (7.4) become comparable. In such a case, one should calculate also the force coefficients $f_{\varphi\sigma}$ and $f_{\varphi\varphi}$, defined in Ref. [8].

In summary, when the particles are large enough, then Eqs. (7.1) and (7.2) are satisfied and the theory developed in the present article is sufficient for a quantitative theoretical description of the electrodipping force, $F^{(el)} \approx F^{(n)}$. In contrast, for smaller particles the deviations from Eqs. (7.1) and (7.2) could become significant, and then one should calculate also $F^{(w)}$, $f_{\varphi\sigma}$, and $f_{\varphi\varphi}$ to achieve an accurate quantitative description. Note that the formalism, developed here for calculation of $f_{\sigma\sigma}$, is directly applicable for the calculation of $f_{\varphi\sigma}$ and $f_{\varphi\varphi}$.

8. Summary and conclusions

Our purpose here is to solve the theoretical problem about the electric field of a charged dielectric particle, which is adsorbed at the water–nonpolar fluid (oil, air) boundary; see Figs. 1 and 2. In accordance with the experimental findings [2, 6,8,11–13], we consider the case when the surface charges are located at the particle–nonpolar fluid boundary. The symmetry of the system suggests the Mehler–Fock integral transform to be used for solving the electrostatic boundary problem (Section 3). In the special case when the dielectric constants of the particle and the nonpolar fluid are equal, the solution is obtained in a closed analytical form (Section 4). In the general case of different dielectric constants, the problem is reduced to the solution of a Fredholm integral equation, Eq. (5.6), which can be carried out numerically, by iterations (Section 5.1 and Appendix C). The latter numerical procedure turns out to be much faster than the procedure for direct numerical integration of the original partial differential equations, which has been previously used [8].

In addition, the derived equations enabled us to obtain analytical expressions for the asymptotic behavior of the electric field near the particle and far from it. The long-range asymptotics indicates that two similar particles repel each other as dipoles, whose dipole moments are expressed through the particle radius, contact angle, dielectric constant and surface charge density (Section 6). On the other hand, the analytical expression for the short-range asymptotics is important, because the electric field has an integrable divergence at the particle contact line that is described by the functions $C(\alpha, \varepsilon_{pn})$ and $\nu(\alpha, \varepsilon_{pn})$; see Eq. (5.18). The knowledge of the short-range asymptotics ensures accurate calculation of the electrodipping-force coefficient, $f_R(\alpha, \varepsilon_{pn})$.

For a fast and convenient application of the results obtained in the present paper, the reader could use the dependencies $D(\alpha, \varepsilon_{pn})$, $C(\alpha, \varepsilon_{pn})$, $f_R(\alpha, \varepsilon_{pn})$, and $\nu(\alpha, \varepsilon_{pn})$, tabulated in Appendix D, instead of repeating the calculations described in Section 5.1 and Appendix C. Thus, $D(\alpha, \varepsilon_{pn})$, $C(\alpha, \varepsilon_{pn})$, and $\nu(\alpha, \varepsilon_{pn})$ can be applied for calculation of the meniscus shape around an adsorbed particle, see Ref. [52]. To do that, we have taken into account the effects of both gravity and electric force on the meniscus shape [52]. $f_R(\alpha, \varepsilon_{pn})$ can be used for computing the electrodipping force, and for determining the surface charge density, σ_{pn}; see Eq. (4.15). $D(\alpha, \varepsilon_{pn})$ is necessary for calculation of the electrostatic interaction between two adsorbed particles at long distances, in accordance with Eqs. (6.2)–(6.4). After a theoretical upgrade, the results could be also applied for prediction of the electric-field-induced capillary attraction [3]. The comparison of the present theory with the experiment can be found in Ref. [52].

Acknowledgments

Appendix A. Analytical solution to the problem for $\alpha \ll 1$

The considered electrostatic problem has a closed analytical solution for $\alpha \ll 1$. Physically, this is the case of hydrophilic particle, whose contact angle is close to zero, see Fig. 2. In this case, our boundary problem, Eqs. (2.1)–(2.3), reduces to

$$\frac{1}{r}\frac{\partial}{\partial r}\left(r\frac{\partial\varphi_k}{\partial r}\right) + \frac{\partial^2\varphi_k}{\partial z^2} = 0 \quad \text{in } \Omega_k \quad (k = \text{n}, \text{p}), \tag{A.1}$$

$$\varphi_n = \varphi_p = 0 \quad (z = 0, \ r \geqslant r_c), \tag{A.2}$$

$$\varphi_n = \varphi_p, \quad \varepsilon_p\frac{\partial\varphi_p}{\partial z} - \varepsilon_n\frac{\partial\varphi_n}{\partial z} = 4\pi\sigma_{pn}$$
$$(z = 0, \ 0 \leqslant r < r_c). \tag{A.3}$$

The solution of Eq. (A.1), which is finite at infinity, and which is continuous at the plane $z = 0$, can be expressed in terms of Hankel transform [36,37,53],

$$\varphi_n = \frac{8\pi\sigma_{pn}}{\varepsilon_n + \varepsilon_p}\int_0^\infty X(s)\exp(-sz)J_0(sr)\,ds,$$

$$\varphi_p = \frac{8\pi\sigma_{pn}}{\varepsilon_n + \varepsilon_p}\int_0^\infty X(s)\exp(sz)J_0(sr)\,ds, \tag{A.4}$$

where J_0 is the Bessel function of zero order, and $X(s)$ is the Hankel image of the electric potential. The substitution of Eq. (A.4) into the boundary conditions, Eqs. (A.2), (A.3), leads to the following integral equations:

$$\int_0^\infty sX(s)J_0(sr)\,ds = \frac{1}{2} \quad \text{at } 0 \leqslant r < r_c,$$

$$\int_0^\infty X(s)J_0(sr)\,ds = 0 \quad \text{at } r \geqslant r_c. \tag{A.5}$$

The exact solution of Eq. (A.5) is reported in Ref. [53]; its application to our specific case yields

$$X(s) = \left(\frac{s}{2\pi}\right)^{1/2}\int_0^{r_c} r^{3/2}J_{1/2}(sr)\,dr. \tag{A.6}$$

Using the fact that $J_{1/2}(x) = [2/(\pi x)]^{1/2}\sin x$ (see, e.g., Refs. [29,40]), we take the integral in Eq. (A.6):

$$X(s) = \frac{1}{\pi s^2}\big[\sin(sr_c) - (sr_c)\cos(sr_c)\big]. \tag{A.7}$$

With the help of Eqs. (A.4) and (A.7), we express the electric field, $E_z|_{z=0} = \partial\varphi_n/\partial z|_{z=0}$:

$$E_z|_{z=0} = \frac{8\sigma_{pn}}{\varepsilon_n + \varepsilon_p}\int_0^\infty \left(\frac{\sin s}{s} - \cos s\right)J_0(sr/r_c)\,ds. \tag{A.8}$$

The integral in Eq. (A.8) can be taken exactly [41],

$$E_z|_{z=0} = -\frac{8\sigma_{pn}}{\varepsilon_n + \varepsilon_p}\left[\frac{x_1}{(1 - x_1^2)^{1/2}} - \arcsin(x_1)\right], \tag{A.9}$$

where, as usual, $x_1 = r_c/r$. At large distances from the particle, $x_1 \ll 1$, we have

$$\frac{x_1}{(1 - x_1^2)^{1/2}} - \arcsin(x_1) = \frac{x_1^3}{3} + \frac{3x_1^5}{10} + \cdots. \tag{A.10}$$

Then, the comparison of Eqs. (A.9) and (5.8) yields an expression for $D|_{\alpha=0}$:

$$D(0, \varepsilon_{pn}) = \frac{2}{3\pi(1 + \varepsilon_{pn})}. \tag{A.11}$$

In the opposite limit, $x_1 \to 1$, close to the contact line we have

$$\frac{x_1}{(1 - x_1^2)^{1/2}} - \arcsin(x_1) = \frac{1}{2^{1/2}(1 - x_1)^{1/2}} - \frac{\pi}{2} + \cdots. \tag{A.12}$$

Then, the comparison of Eqs. (A.9) and (5.18) yields an expression for $C|_{\alpha=0}$,

$$C(0, \varepsilon_{pn}) = \frac{2^{1/2}}{\pi(1 + \varepsilon_{pn})}, \tag{A.13}$$

where at the last step we have used the fact that $\nu|_{\alpha=0} = 0.5$; see Fig. 9. Equations (A.11) and (A.13) give the values of the parameters D and C for small contact angles; see also Figs. 8 and 10 and Tables 1 and 2 in Appendix D. In addition, because $f_{\sigma\sigma}$ is proportional to integral over $E_z^2|_{z=0}$, see Eq. (5.20), Eq. (A.9) shows that $f_{\sigma\sigma}$ has logarithmic singularity at $\alpha \to 0$. Finally, comparing Eqs. (A.9) and (3.22), we obtain

$$J(x_1, 0, \varepsilon_{pn}) = \frac{2(1 - x_1)^{1/2}}{\pi(1 + \varepsilon_{pn})x_1^3}\left[\frac{x_1}{(1 - x_1^2)^{1/2}} - \arcsin(x_1)\right]. \tag{A.14}$$

Appendix B. Calculation of the integral in Eq. (4.2)

To transform the integral in Eq. (4.2), we substitute $K(\eta, \tau)$ from Eqs. (3.7) and (3.9):

$$I_e(\eta, \alpha) = \frac{4}{\pi\sin\alpha}\int_\eta^\infty \frac{dy}{(\cosh y - \cosh\eta)^{1/2}}$$
$$\times \int_0^\infty \frac{\sinh[(\pi - \xi_c)\tau]}{\sinh[(\pi + \xi_c)\tau]}\sin(\tau y)\tau\,d\tau. \tag{B.1}$$

The last integral in Eq. (B.1) is of Fourier type and it can be taken exactly,

$$\int_0^\infty \frac{\sinh[(\pi - \xi_c)\tau]}{\sinh[(\pi + \xi_c)\tau]}\sin(\tau y)\tau\,d\tau$$
$$= \frac{\nu_e^2\sin(2\nu_e\xi_c)\sinh(\nu_e y)}{2[\cosh(\nu_e y) - \cos(2\nu_e\xi_c)]^2}, \tag{B.2}$$

Table 1
Function $D(\alpha, \varepsilon_{\mathrm{pn}})$ defined by Eq. (5.9)

α	$\varepsilon_{\mathrm{pn}} = \varepsilon_{\mathrm{p}}/\varepsilon_{\mathrm{n}}$								
	0.125	0.250	0.500	0.750	1.00	1.50	2.00	4.00	8.00
0	0.1886	0.1698	0.1415	0.1213	0.1061	0.08488	0.07074	0.04244	0.02358
5	0.1941	0.1755	0.1472	0.1268	0.1114	0.08957	0.07490	0.04525	0.02526
10	0.2006	0.1822	0.1539	0.1332	0.1174	0.09490	0.07964	0.04846	0.02718
15	0.2083	0.1900	0.1615	0.1405	0.1243	0.1010	0.08505	0.05214	0.02939
20	0.2173	0.1990	0.1702	0.1488	0.1321	0.1079	0.09123	0.05636	0.03194
25	0.2277	0.2093	0.1803	0.1583	0.1411	0.1159	0.09831	0.06122	0.03489
30	0.2398	0.2213	0.1917	0.1692	0.1513	0.1250	0.1065	0.06682	0.03831
35	0.2538	0.2351	0.2049	0.1817	0.1631	0.1355	0.1158	0.07333	0.04229
40	0.2700	0.2511	0.2202	0.1960	0.1767	0.1476	0.1267	0.08090	0.04696
45	0.2888	0.2695	0.2378	0.2127	0.1924	0.1616	0.1393	0.08976	0.05246
50	0.3107	0.2910	0.2582	0.2320	0.2107	0.1780	0.1541	0.1002	0.05897
55	0.3363	0.3160	0.2820	0.2546	0.2320	0.1971	0.1714	0.1125	0.06673
60	0.3664	0.3454	0.3099	0.2811	0.2571	0.2197	0.1918	0.1272	0.07604
65	0.4018	0.3800	0.3428	0.3123	0.2868	0.2465	0.2162	0.1449	0.08730
70	0.4438	0.4211	0.3819	0.3494	0.3221	0.2785	0.2453	0.1662	0.1010
75	0.4941	0.4701	0.4286	0.3939	0.3644	0.3170	0.2805	0.1921	0.1179
80	0.5546	0.5292	0.4850	0.4477	0.4157	0.3638	0.3234	0.2241	0.1388
85	0.6281	0.6011	0.5537	0.5132	0.4783	0.4211	0.3761	0.2637	0.1651
90	0.7184	0.6894	0.6381	0.5939	0.5556	0.4921	0.4417	0.3135	0.1985
95	0.8306	0.7992	0.7432	0.6946	0.6521	0.5811	0.5241	0.3768	0.2413
100	0.9718	0.9374	0.8757	0.8217	0.7742	0.6941	0.6292	0.4583	0.2973
105	1.152	1.114	1.045	0.9848	0.9311	0.8398	0.7651	0.5649	0.3713
110	1.386	1.344	1.266	1.197	1.136	1.031	0.9438	0.7067	0.4712
115	1.696	1.648	1.559	1.480	1.409	1.286	1.183	0.8990	0.6086
120	2.116	2.060	1.956	1.864	1.780	1.635	1.512	1.166	0.8020
125	2.700	2.633	2.510	2.400	2.299	2.123	1.974	1.545	1.082
130	3.536	3.455	3.305	3.170	3.047	2.830	2.644	2.102	1.499
135	4.781	4.679	4.491	4.320	4.165	3.889	3.652	2.950	2.145
140	6.720	6.587	6.341	6.117	5.913	5.551	5.237	4.298	3.192
145	9.916	9.733	9.395	9.088	8.808	8.309	7.875	6.566	4.986
150	15.59	15.32	14.83	14.38	13.96	13.23	12.60	10.67	8.294
155	26.71	26.28	25.48	24.76	24.10	22.94	21.93	18.85	15.01
160	51.81	51.02	49.56	48.25	47.05	44.93	43.11	37.58	30.67
165	122.2	120.4	117.1	114.2	111.5	106.8	102.8	90.72	75.84
170	410.7	404.9	394.3	384.8	376.2	361.2	348.4	310.7	265.4
175	3274	3228	3145	3071	3005	2889	2790	2505	2175

where ν_{e} is defined by Eq. (4.4). Substituting Eq. (B.2) into Eq. (B.1), we obtain

$$I_{\mathrm{e}} = \frac{2\nu_{\mathrm{e}} \sin(2\nu_{\mathrm{e}}\xi_{\mathrm{c}})}{(\pi + \xi_{\mathrm{c}}) \sin\alpha} \int_{\eta}^{\infty} \frac{(\cosh y - \cosh\eta)^{-1/2} \sinh(\nu_{\mathrm{e}} y)}{[\cosh(\nu_{\mathrm{e}} y) - \cos(2\nu_{\mathrm{e}}\xi_{\mathrm{c}})]^2} \, dy.$$

(B.3)

Finally, in Eq. (B.3) we introduce a new integration variable, $y = 2x + \eta$, and after some transformations we derive Eq. (4.3).

Appendix C. Procedure for fast calculation of the kernels K and U

For a fast computation of the kernel $K(\eta, \tau)$, defined by Eq. (3.9), we have been using two alternative expressions, depending on whether η is small or large. For small values of η, it is convenient to use Eq. (8.11.1) in Ref. [40],

$$K(\eta, \tau) = F_{2,1}\left(\frac{1}{2}, b; 1; y\right) \exp(-b\eta),$$

(C.1)

where

$$b = 0.5 + i\tau, \qquad y = 1 - \exp(-2\eta),$$

(C.2)

and $F_{2,1}(a, b; c; y)$ is the hypergeometric function. On the other hand, for large values of η, it is more convenient to use Eq. (15.3.6) in Ref. [40],

$$K(\eta, \tau) = F_{2,1}\left(\frac{1}{2}, b; c; 1 - y\right) \frac{\Gamma(-i\tau) \exp(-b\eta)}{\Gamma(\bar{b})\pi^{1/2}}$$
$$+ F_{2,1}\left(\frac{1}{2}, \bar{b}; \bar{c}; 1 - y\right) \frac{\Gamma(i\tau) \exp(-\bar{b}\eta)}{\Gamma(b)\pi^{1/2}},$$

(C.3)

where Γ is the gamma function; b and y are given by Eq. (C.2), and the other parameters are

$$\bar{b} = 0.5 - i\tau, \qquad c = 1 + i\tau, \qquad \bar{c} = 1 - i\tau.$$

(C.4)

In our computations, we used FORTRAN with IMSL, where the Γ function of complex argument is a built-in function. To calculate $F_{2,1}(a, b; c; y)$, we applied numerical summation of the standard hypergeometric series of Gauss [40]. For the

Table 2
Function $C(\alpha, \varepsilon_{pn})$ defined by Eq. (5.19)

α	$\varepsilon_{pn} = \varepsilon_p/\varepsilon_n$								
	0.125	0.250	0.500	0.750	1.00	1.50	2.00	4.00	8.00
0	0.4001	0.3601	0.3001	0.2572	0.2251	0.1801	0.1501	0.09003	0.05002
5	0.4170	0.3740	0.3101	0.2648	0.2328	0.1843	0.1532	0.09152	0.05070
10	0.4401	0.3930	0.3238	0.2755	0.2413	0.1904	0.1580	0.09400	0.05195
15	0.4669	0.4145	0.3391	0.2872	0.2507	0.1972	0.1633	0.09680	0.05340
20	0.4977	0.4390	0.3561	0.3001	0.2610	0.2047	0.1691	0.09996	0.05507
25	0.5334	0.4667	0.3749	0.3143	0.2723	0.2129	0.1756	0.1035	0.05698
30	0.5747	0.4980	0.3958	0.3299	0.2847	0.2219	0.1827	0.1075	0.05916
35	0.6224	0.5333	0.4187	0.3469	0.2982	0.2318	0.1905	0.1120	0.06166
40	0.6777	0.5732	0.4441	0.3655	0.3130	0.2426	0.1992	0.1171	0.06451
45	0.7417	0.6181	0.4719	0.3859	0.3292	0.2546	0.2088	0.1227	0.06777
50	0.8159	0.6683	0.5023	0.4081	0.3469	0.2677	0.2195	0.1292	0.07150
55	0.9017	0.7244	0.5355	0.4322	0.3662	0.2822	0.2313	0.1364	0.07577
60	1.000	0.7864	0.5715	0.4585	0.3873	0.2981	0.2445	0.1447	0.08067
65	1.113	0.8543	0.6105	0.4870	0.4104	0.3158	0.2592	0.1540	0.08632
70	1.238	0.9275	0.6522	0.5178	0.4357	0.3354	0.2756	0.1647	0.09285
75	1.374	1.005	0.6966	0.5511	0.4632	0.3571	0.2941	0.1770	0.1004
80	1.515	1.084	0.7434	0.5869	0.4934	0.3813	0.3148	0.1910	0.1093
85	1.650	1.162	0.7920	0.6254	0.5263	0.4083	0.3383	0.2073	0.1197
90	1.763	1.236	0.8420	0.6664	0.5623	0.4385	0.3649	0.2262	0.1320
95	1.840	1.300	0.8925	0.7101	0.6017	0.4724	0.3952	0.2482	0.1467
100	1.870	1.350	0.9427	0.7565	0.6447	0.5105	0.4298	0.2742	0.1643
105	1.851	1.384	0.9915	0.8053	0.6916	0.5537	0.4696	0.3050	0.1857
110	1.793	1.400	1.038	0.8564	0.7429	0.6025	0.5156	0.3418	0.2119
115	1.710	1.401	1.082	0.9098	0.7987	0.6580	0.5689	0.3862	0.2445
120	1.617	1.389	1.118	0.9562	0.8596	0.7213	0.6313	0.4403	0.2854
125	1.523	1.366	1.158	1.018	0.9257	0.7938	0.7046	0.5071	0.3378
130	1.440	1.345	1.191	1.081	0.9975	0.8771	0.7915	0.5906	0.4060
135	1.364	1.316	1.220	1.143	1.075	0.9726	0.8948	0.6964	0.4968
140	1.298	1.285	1.246	1.205	1.159	1.084	1.019	0.8332	0.6205
145	1.242	1.255	1.268	1.267	1.249	1.210	1.168	1.013	0.7941
150	1.199	1.234	1.289	1.329	1.345	1.355	1.349	1.255	1.047
155	1.163	1.219	1.313	1.391	1.446	1.530	1.575	1.591	1.433
160	1.136	1.204	1.334	1.454	1.553	1.711	1.836	2.065	2.053
165	1.116	1.197	1.357	1.516	1.664	1.936	2.167	2.767	3.134
170	1.102	1.193	1.384	1.578	1.777	2.176	2.554	3.813	5.206
175	1.099	1.190	1.413	1.640	1.890	2.412	2.967	5.322	8.384

process of computations, it is convenient to introduce the quantity

$$\eta_b \equiv 0.1371 + 0.202 \exp(-0.0312\tau). \tag{C.5}$$

To minimize the number of terms summed when calculating the hypergeometric series, we used the following criterion: For $0 \leqslant \eta \leqslant \eta_b$, $K(\eta, \tau)$ is calculated by means of Eq. (C.1), whereas for $\eta > \eta_b$, $K(\eta, \tau)$ is calculated by means of Eq. (C.3). Alternatively, one could use the software "Mathematica 5.0," where $F_{2,1}(a, b; c; y)$ is a built-in function.

To compute the function $U(\tau, \tilde{\tau})$, we carried out the integration in Eq. (5.4) numerically, by using the Simpson rule. Equation (C.3) shows that the function $K(\eta, \tau)K(\eta, \tilde{\tau})$ decays as $\exp(-\eta)$ at large η, and therefore the integral in Eq. (5.4) converges very well.

Appendix D. Tabulated values of the computed basic functions

For a fast and convenient application of the results obtained in the present paper, the reader could use the dependencies

$D(\alpha, \varepsilon_{pn})$, $C(\alpha, \varepsilon_{pn})$, $f_R(\alpha, \varepsilon_{pn})$, and $\nu(\alpha, \varepsilon_{pn})$, given in Tables 1, 2, 3, and 4, instead of repeating the calculations described in Section 5.1 and Appendix C.

Let $f(\alpha, \varepsilon_{pn})$ be either of the above four tabulated functions. We are interested to obtain its value for a given $\alpha_1 < \alpha < \alpha_2$ and $\varepsilon_1 < \varepsilon_{pn} < \varepsilon_2$, where α_1, α_2, ε_1, and ε_2 are values given in the respective table. Then, $f(\alpha, \varepsilon_{pn})$ can be calculated by means of the following four-point interpolation formula:

$$\begin{aligned}
f(\alpha, \varepsilon_{pn}) =& \frac{(\alpha - \alpha_2)(\varepsilon_{pn} - \varepsilon_2)}{(\alpha_1 - \alpha_2)(\varepsilon_1 - \varepsilon_2)} f(\alpha_1, \varepsilon_1) \\
&+ \frac{(\alpha - \alpha_2)(\varepsilon_{pn} - \varepsilon_1)}{(\alpha_1 - \alpha_2)(\varepsilon_2 - \varepsilon_1)} f(\alpha_1, \varepsilon_2) \\
&+ \frac{(\alpha - \alpha_1)(\varepsilon_{pn} - \varepsilon_2)}{(\alpha_2 - \alpha_1)(\varepsilon_1 - \varepsilon_2)} f(\alpha_2, \varepsilon_1) \\
&+ \frac{(\alpha - \alpha_1)(\varepsilon_{pn} - \varepsilon_1)}{(\alpha_2 - \alpha_1)(\varepsilon_2 - \varepsilon_1)} f(\alpha_2, \varepsilon_2).
\end{aligned} \tag{D.1}$$

Appendix E. Symbol definitions

A_{pn} area of the particle–nonpolar fluid interface, Eq. (6.5)

Table 3
Function $f_R(\alpha, \varepsilon_{pn}) = f_{\sigma\sigma} \sin^2\alpha$ defined by Eq. (4.13)

α	$\varepsilon_{pn} = \varepsilon_p/\varepsilon_n$								
	0.125	0.250	0.500	0.750	1.00	1.50	2.00	4.00	8.00
0	0.0	0.0	0.0	0.0	0.0	0.0	0.0	0.0	0.0
5	0.1482	0.1342	0.1129	0.09740	0.08565	0.06901	0.05778	0.03500	0.01957
10	0.2878	0.2622	0.2225	0.1933	0.1708	0.1386	0.1166	0.07132	0.04014
15	0.4196	0.3843	0.3291	0.2877	0.2555	0.2088	0.1765	0.1091	0.06183
20	0.5440	0.5011	0.4327	0.3807	0.3399	0.2798	0.2377	0.1484	0.08475
25	0.6618	0.6128	0.5337	0.4726	0.4239	0.3516	0.3002	0.1895	0.1090
30	0.7734	0.7198	0.6321	0.5632	0.5078	0.4243	0.3643	0.2325	0.1349
35	0.8792	0.8224	0.7280	0.6528	0.5916	0.4980	0.4299	0.2777	0.1625
40	0.9797	0.9209	0.8217	0.7415	0.6754	0.5730	0.4974	0.3253	0.1921
45	1.075	1.016	0.9133	0.8294	0.7593	0.6493	0.5669	0.3756	0.2240
50	1.166	1.106	1.003	0.9165	0.8435	0.7271	0.6386	0.4289	0.2585
55	1.253	1.194	1.091	1.003	0.9280	0.8066	0.7128	0.4856	0.2960
60	1.335	1.278	1.177	1.089	1.013	0.8879	0.7897	0.5462	0.3370
65	1.414	1.360	1.261	1.175	1.099	0.9713	0.8696	0.6111	0.3821
70	1.489	1.438	1.344	1.260	1.185	1.057	0.9529	0.6809	0.4318
75	1.561	1.514	1.426	1.345	1.272	1.145	1.040	0.7563	0.4869
80	1.630	1.587	1.506	1.430	1.360	1.236	1.131	0.8380	0.5485
85	1.695	1.658	1.585	1.515	1.449	1.330	1.226	0.9269	0.6177
90	1.758	1.727	1.663	1.600	1.540	1.427	1.326	1.024	0.6958
95	1.818	1.793	1.740	1.685	1.631	1.527	1.431	1.130	0.7847
100	1.875	1.857	1.815	1.770	1.724	1.631	1.542	1.248	0.8864
105	1.930	1.918	1.890	1.856	1.818	1.739	1.660	1.377	1.004
110	1.982	1.978	1.963	1.941	1.914	1.852	1.784	1.521	1.140
115	2.031	2.035	2.035	2.026	2.011	1.968	1.915	1.681	1.299
120	2.078	2.091	2.106	2.112	2.110	2.090	2.054	1.859	1.488
125	2.123	2.144	2.176	2.197	2.210	2.216	2.202	2.060	1.712
130	2.165	2.194	2.244	2.282	2.311	2.346	2.359	2.285	1.980
135	2.204	2.242	2.310	2.367	2.413	2.482	2.524	2.540	2.306
140	2.240	2.288	2.375	2.450	2.516	2.622	2.700	2.828	2.705
145	2.273	2.330	2.436	2.532	2.618	2.766	2.884	3.153	3.198
150	2.303	2.369	2.495	2.611	2.719	2.912	3.076	3.521	3.811
155	2.329	2.405	2.550	2.687	2.818	3.059	3.277	3.935	4.580
160	2.352	2.436	2.599	2.758	2.911	3.204	3.477	4.394	5.548
165	2.371	2.462	2.642	2.821	2.996	3.341	3.675	4.893	6.763
170	2.385	2.482	2.677	2.873	3.069	3.462	3.856	5.410	8.252
175	2.393	2.494	2.697	2.902	3.110	3.532	3.963	5.890	9.941
180	2.397	2.500	2.710	2.923	3.142	3.592	4.062	6.130	11.10

B_n, B_p transforms of Ψ_n, Ψ_p, Eq. (3.8)
C value of J at the contact line, Eq. (5.18)
C_e the value of C at $\varepsilon_p = \varepsilon_n$; see Eq. (4.12)
D dipole moment coefficient, Eqs. (5.9) and (6.2)
D_e the value of D at $\varepsilon_p = \varepsilon_n$; see Eq. (4.6)
E_x, E_z components of the electric-field intensity
$f(\alpha, \varepsilon_{pn})$ coefficient of the electrodipping force, Eq. (4.15)
$f_R(\alpha, \varepsilon_{pn})$ force coefficient, Eq. (4.15)
$f_{\sigma\sigma}(\alpha, \varepsilon_{pn})$ force coefficient, Eqs. (2.13) and (4.15)
$f_{\varphi\sigma}, f_{\varphi\varphi}$ force coefficients, Eq. (7.3)
F_{12} interaction force between two dipoles, Eq. (6.3)
$F^{(el)}$ electrodipping force acting on the particle, Eq. (1.1)
$F^{(n)}$ contribution to $F^{(el)}$ due to charges at S_{pn}, Eq. (4.15)
$F^{(w)}$ contribution to $F^{(el)}$ due to charges at S_{pw}, Eq. (1.1)
g acceleration due to gravity
h, h_ξ, h_η metric coefficients, Eqs. (2.4), (2.5)
I integral defined by Eq. (3.17)
I_e the value of I at $\varepsilon_p = \varepsilon_n$; see Eq. (4.2)
J function of bounded variation, Eq. (3.23)

$J_0, J_{1/2}$ Bessel functions, Appendix A
$K(\eta, \tau)$ kernel of the integral transform, Eq. (3.9)
L distance between two particles, Eq. (6.3)
$L[\Psi]$ linear differential operator, Eq. (3.3)
p_d dipole moment, Eqs. (6.1), (6.2)
p_{el} pressure of electric origin acting at S_{nw}
$P_\nu(u)$ Legendre function of the first kind
q inverse capillary length, Eq. (1.3)
r radial cylindrical coordinate
r_c radius of the contact line, Fig. 2
R particle radius, Fig. 1
S_{nw} nonpolar fluid–water interface, Fig. 2
S_{pn} particle–nonpolar fluid interface, Fig. 2
S_{pw} particle–water interface, Fig. 2
u variable, $u = \cosh\eta$
U_{12} interaction energy between two dipoles, Eq. (6.4)
$U(\tau, \tilde{\tau})$ kernel in Eq. (5.1)
x_1 dimensionless coordinate, Eq. (3.19)
z vertical cylindrical coordinate

Table 4
Function $\nu(\alpha, \varepsilon_{pn})$ defined as the smallest positive root of Eq. (5.17)

α	$\varepsilon_{pn} = \varepsilon_p/\varepsilon_n$								
	0.125	0.250	0.500	0.750	1.00	1.50	2.00	4.00	8.00
0	0.5000	0.5000	0.5000	0.5000	0.5000	0.5000	0.5000	0.5000	0.5000
5	0.5127	0.5114	0.5094	0.5081	0.5070	0.5056	0.5047	0.5028	0.5015
10	0.5260	0.5232	0.5192	0.5164	0.5143	0.5114	0.5094	0.5056	0.5031
15	0.5400	0.5357	0.5294	0.5250	0.5217	0.5173	0.5143	0.5085	0.5047
20	0.5547	0.5487	0.5399	0.5339	0.5294	0.5233	0.5193	0.5114	0.5063
25	0.5703	0.5623	0.5509	0.5430	0.5373	0.5295	0.5244	0.5144	0.5079
30	0.5867	0.5766	0.5623	0.5525	0.5455	0.5358	0.5296	0.5175	0.5096
35	0.6040	0.5915	0.5741	0.5623	0.5538	0.5424	0.5349	0.5206	0.5113
40	0.6222	0.6071	0.5863	0.5725	0.5625	0.5491	0.5405	0.5238	0.5131
45	0.6414	0.6235	0.5990	0.5829	0.5714	0.5560	0.5461	0.5271	0.5149
50	0.6617	0.6405	0.6122	0.5937	0.5806	0.5632	0.5520	0.5305	0.5167
55	0.6830	0.6582	0.6258	0.6049	0.5902	0.5706	0.5580	0.5340	0.5187
60	0.7052	0.6766	0.6398	0.6164	0.6000	0.5782	0.5643	0.5377	0.5207
65	0.7285	0.6956	0.6543	0.6283	0.6102	0.5861	0.5708	0.5416	0.5228
70	0.7524	0.7151	0.6692	0.6406	0.6207	0.5944	0.5776	0.5456	0.5250
75	0.7769	0.7351	0.6845	0.6533	0.6316	0.6029	0.5847	0.5498	0.5274
80	0.8015	0.7552	0.7002	0.6663	0.6429	0.6119	0.5922	0.5543	0.5299
85	0.8256	0.7753	0.7161	0.6798	0.6545	0.6212	0.6000	0.5590	0.5326
90	0.8485	0.7952	0.7323	0.6936	0.6667	0.6310	0.6082	0.5641	0.5354
95	0.8697	0.8145	0.7486	0.7078	0.6792	0.6413	0.6169	0.5695	0.5385
100	0.8886	0.8330	0.7650	0.7224	0.6923	0.6521	0.6261	0.5753	0.5419
105	0.9050	0.8505	0.7815	0.7373	0.7059	0.6635	0.6359	0.5817	0.5456
110	0.9190	0.8667	0.7978	0.7526	0.7200	0.6756	0.6465	0.5885	0.5497
115	0.9308	0.8817	0.8140	0.7682	0.7347	0.6885	0.6578	0.5961	0.5542
120	0.9407	0.8955	0.8300	0.7841	0.7500	0.7022	0.6700	0.6045	0.5593
125	0.9491	0.9080	0.8456	0.8004	0.7660	0.7169	0.6834	0.6139	0.5651
130	0.9564	0.9194	0.8609	0.8169	0.7826	0.7327	0.6980	0.6245	0.5718
135	0.9627	0.9299	0.8759	0.8337	0.8000	0.7497	0.7140	0.6366	0.5796
140	0.9682	0.9395	0.8905	0.8508	0.8182	0.7682	0.7318	0.6506	0.5889
145	0.9732	0.9484	0.9048	0.8681	0.8372	0.7884	0.7518	0.6671	0.6002
150	0.9777	0.9567	0.9187	0.8858	0.8571	0.8104	0.7742	0.6868	0.6142
155	0.9818	0.9645	0.9325	0.9037	0.8780	0.8347	0.7998	0.7109	0.6323
160	0.9858	0.9720	0.9460	0.9220	0.9000	0.8614	0.8290	0.7410	0.6566
165	0.9895	0.9792	0.9594	0.9407	0.9231	0.8910	0.8629	0.7798	0.6909
170	0.9930	0.9862	0.9728	0.9598	0.9474	0.9238	0.9021	0.8316	0.7432
175	0.9965	0.9931	0.9863	0.9796	0.9730	0.9601	0.9477	0.9027	0.8322
180	1.000	1.000	1.000	1.000	1.000	1.000	1.000	1.000	1.000

Greek symbols

α	central angle determining particle position, Fig. 2
β	parameter defined by Eq. (5.3)
γ	interfacial tension of S_{nw}, Figs. 1 and 2
Γ	gamma function
ε_n	dielectric constant of the nonpolar fluid
ε_p	dielectric constant of the particle
ε_{pn}	dielectric constant ratio, $\varepsilon_{pn} = \varepsilon_p/\varepsilon_n$
$\zeta(r)$	meniscus profile, Eq. (1.3)
η	toroidal coordinate, Eq. (2.4)
μ	parameter in Eq. (1.4); $\mu = 1 - 2(1 - \nu)$
ν	parameter in Eq. (3.22) defined by Eq. (5.17)
ν_e	the value of ν at $\varepsilon_p = \varepsilon_n$; see Eq. (4.4)
ξ	toroidal coordinate, Eq. (2.4)
ξ_c	value of ξ at the contact line, $\xi_c = \pi - \alpha$
σ_{pn}	surface electric charge density at S_{pn}
τ	variable in the Mehler–Fock transform, Eq. (3.5)
φ_n	electric potential in the nonpolar fluid
φ_p	electric potential in the particle

Φ_n, Φ_p	dimensionless potentials, Eq. (2.8)
Ψ_n, Ψ_p	dimensionless potentials, Eq. (3.1)
$\Psi_s(\tau)$	image of the dimensionless electric potential at S_{pn}, Eq. (3.12)
Ω_n, Ω_p	spatial domains, Eq. (2.1)

References

[1] R. Aveyard, J.H. Clint, D. Nees, V.N. Paunov, Langmuir 16 (2000) 1969–1979.

[2] R. Aveyard, B.P. Binks, J.H. Clint, P.D.I. Fletcher, T.S. Horozov, B. Neumann, V.N. Paunov, J. Annesley, S.W. Botchway, D. Nees, A.W. Parker, A.D. Ward, A. Burgess, Phys. Rev. Lett. 88 (2002) 246102.

[3] M.G. Nikolaides, A.R. Bausch, M.F. Hsu, A.D. Dinsmore, M.P. Brenner, C. Gay, D.A. Weitz, Nature 420 (2002) 299–301.

[4] M. Megens, J. Aizenberg, Nature 424 (2003) 1014.

[5] D. Langevin, Chem. Phys. Phys. Chem. 4 (2003) 1057–1058.

[6] T.S. Horozov, R. Aveyard, J.H. Clint, B.P. Binks, Langmuir 19 (2003) 2822–2829.

[7] E.J. Stancik, M. Kouhkan, G.G. Fuller, Langmuir 20 (2004) 90–94.

[8] K.D. Danov, P.A. Kralchevsky, M.P. Boneva, Langmuir 20 (2004) 6139–6151.

[9] M. Oettel, A. Domínguez, S. Dietrich, Phys. Rev. E 71 (2005) 051401.

[10] A. Würger, L. Foret, J. Phys. Chem. B 109 (2005) 16435–16438.
[11] T.S. Horozov, R. Aveyard, J.H. Clint, Langmuir 21 (2005) 2330–2341.
[12] T.S. Horozov, R. Aveyard, B.P. Binks, J.H. Clint, Langmuir 21 (2005) 7407–7412.
[13] T.S. Horozov, B.P. Binks, Colloids Surf. A 267 (2005) 64–73.
[14] J.C. Fernández-Toledano, A. Moncho-Jordá, F. Martínez-López, R. Hidalgo-Álvarez, Langmuir 20 (2004) 6977–6980.
[15] I.I. Smalyukh, S. Chernyshuk, B.I. Lev, A.B. Nych, U. Ognysta, V.G. Nazarenko, O.D. Lavrentovich, Phys. Rev. Lett. 93 (2004) 117801.
[16] L.E. Helseth, R.M. Muruganathan, Y. Zhang, T.M. Fischer, Langmuir 21 (2005) 7271–7275.
[17] B.P. Binks, Curr. Opin. Colloid Interface Sci. 7 (2002) 21–41.
[18] R. Aveyard, B.P. Binks, J.H. Clint, Adv. Colloid Interface Sci. 100–102 (2003) 503–546.
[19] S. Tarimala, L.L. Dai, Langmuir 20 (2004) 3492–3494.
[20] P.A. Kralchevsky, I.B. Ivanov, K.P. Ananthapadmanabhan, A. Lips, Langmuir 21 (2005) 50–63.
[21] K.D. Danov, P.A. Kralchevsky, K.P. Ananthapadmanabhan, A. Lips, Langmuir 22 (2006) 106–115.
[22] O.D. Velev, K. Furusawa, K. Nagayama, Langmuir 12 (1996) 2374–2384.
[23] A.D. Dinsmore, M.F. Hsu, M.G. Nikolaides, M. Marquez, A.R. Bausch, D.A. Weitz, Science 298 (2002) 1006–1009.
[24] M.F. Hsu, M.G. Nikolaides, A.D. Dinsmore, A.R. Bausch, V.D. Gordon, X. Chen, J.W. Hutchinson, D.A. Weitz, M. Marquez, Langmuir 21 (2005) 2963–2970.
[25] P.A. Kralchevsky, K. Nagayama, Adv. Colloid Interface Sci. 85 (2000) 145–192.
[26] M.M. Muller, M. Deserno, A. Guven, Europhys. Lett. 69 (2005) 482–488.
[27] C.A.J. Fletcher, Computational Techniques for Fluid Dynamics 1. Fundamental and General Techniques, second ed., Springer-Verlag, Berlin, 1991, pp. 251–271.
[28] L.D. Landau, E.M. Lifshitz, Electrodynamics of Continuous Media, Course of Theoretical Physics, vol. 8, Pergamon Press, Oxford, 1960.
[29] G.A. Korn, T.M. Korn, Mathematical Handbook, McGraw–Hill, New York, 1968.
[30] G. Arfken, Mathematical Methods for Physicists, Academic Press, Orlando, FL, 1970.
[31] P. Moon, D.E. Spencer, Field Theory Handbook, Including Coordinate Systems, Differential Equations, and Their Solutions, Springer-Verlag, New York, 1988.
[32] N.N. Lebedev, I.P. Skalskaya, Y.S. Uflyand, Problems of Mathematical Physics, Prentice Hall, London, 1965.
[33] F.G. Mehler, Math. Ann. 18 (1881) 161–194.
[34] V.A. Fock, Dokl. Akad. Nauk SSSR 39 (1943) 253–256.
[35] I.N. Sneddon, The Use of Integral Transforms, McGraw–Hill, New York, 1972.
[36] V.A. Ditkin, A.P. Prudnikov, Integral Transforms and Operational Calculus, Pergamon Press, Oxford, 1965.
[37] Yu.A. Brychkov, A.P. Prudnikov, Integral Transforms of Generalized Functions, CRC Press, Boca Raton, FL, 1989.
[38] S.B. Yakubovich, Index Transforms, World Scientific, Singapore, 1996.
[39] E. Janke, F. Emde, F. Lösch, Tables of Higher Functions, McGraw–Hill, New York, 1960.
[40] M. Abramowitz, I.A. Stegun, Handbook of Mathematical Functions, Dover, New York, 1965.
[41] I.S. Gradshteyn, I.M. Ryzhik, Table of Integrals, Series and Products, fifth ed., Academic Press, New York, 1994.
[42] R. Le Ny, J. Phys. A Math. Gen. 14 (1981) 945–955.
[43] H.N. Glaeske, A. Hess, Math. Nachr. 131 (1987) 107–117;
H.N. Glaeske, A. Hess, Math. Nachr. 136 (1988) 119–129.
[44] N. Hayek, B.J. González, Bull. Soc. R. Sci. Liège 61 (1992) 315–327.
[45] B.J. González, E.R. Negrin, Proc. Amer. Math. Soc. 125 (1997) 3243–3253.
[46] N.N. Lebedev, I.P. Skalskaya, Sov. Phys. Tech. Phys. 7 (1962) 268–270.
[47] A. Passian, A. Wig, F. Meriaudeau, T.L. Ferrell, J. Vac. Sci. Technol. B 20 (2002) 76–80.
[48] N.N. Lebedev, Special Functions and Their Applications, Prentice Hall, London, 1965.
[49] A.P. Prudnikov, Yu.A. Brychkov, O.I. Marichev, Integrals and Series, vol. 1, Elementary Functions, CRC Press, Boca Raton, FL, 1998.
[50] P.P. Zabreiko, A.I. Koshelev, M.A. Krasnosel'skii, S.G. Mikhlin, L.S. Rakovshchik, V.Ya. Stetsenko, Integral Equations, Nauka, Moscow, 1968 (in Russian).
[51] K.E. Atkinson, A Survey of Numerical Methods for the Solution of Fredholm Integral Equations of the Second Kind, SIAM, Philadelphia, 1976.
[52] K.D. Danov, P.A. Kralchevsky, M.P. Boneva, Langmuir (2005), submitted for publication.
[53] V.D. Kupradze, T.G. Gegelia, M.O. Basheleishvili, T.V. Burchuladze, Three-Dimensional Problems of the Mathematical Theory of Elasticity and Thermoelasticity, North-Holland, Amsterdam, 1979.